Very low frequency electromagnetic emissions observed with the O.N.R./S.U.I. satellite Injun III

Gurnett, Donald A.

30

VERY LOW FREQUENCY ELECTROMAGNETIC EMISSIONS OBSERVED WITH THE O.N.R./S.U.I. SATELLITE INJUN III

by

Donald A. Gurnett

A thesis submitted in partial fulfillment of the requirements for the degree of Master of Science in the Department of Physics and Astronomy in the Graduate College of the State University of Iowa

August 1963

Chairman: Assistant Professor H. Leinbach

ACKNOWLEDGEMENTS

The support for the Injun III project, of which the VLF experiment was a closely integrated part, was provided in large part by the Office of Naval Research under Contract N9onr-93803. We are particularly thankful to Dr. J. Fregeau of ONR for these arrangements and to him and to Mr. M. Votaw of the Naval Research Laboratory for the opportunity of flying the satellite on a U. S. Navy Bureau of Naval Weapons vehicle.

Telemetry reception was obtained in part through the cooperation of Mr. R. Tetrick of the Goddard Space Flight Center, Dr. R. Rettie of the Canadian National Research Council, and J. Rogers of Salisbury, Southern Rhodesia.

The author sincerely thanks Professor B. J. O'Brien for his stimulation and guidance in all phases of this project, Professor J. A. Van Allen for his assistance and interest in the interpretation of the measurements, and Dr. H. Leinbach for his advice.

The author also wishes to thank Dr. R. M. Gallet and Messrs. R. L. Hanes and J. M. Watts of the National Bureau of Standards for their suggestions in regard to the experiment. Dr. F. S. Atchison of the Naval Ordnance Laboratory of Corona, California has kindly made available the N.O.L. Rayspan spectrum analyzer for extended periods.

Thanks are also extended to Mr. C. Laughlin for his advice as project manager, to Messrs. G. Frohwein, C. Kime, M. Risk, S. Clark, J. Huff, G. Arrendondo, and G. Crossett for their invaluable assistance on the electronics, to Messrs. L. Frank and J. Craven for their assistance in the interpretation of the geiger counter data, to Messrs. H. Taylor and J. Gardner for their assistance in the interpretation of the photometer data, and to Miss R. Rogers and Mrs. D. Walker for their part in analyzing the VLF data.

Thanks are also extended to Messrs. T. Baker, R. Bradley, and G. Jamieson of the Raytheon Company for their work on the satellite-borne spectrum analyzer, to

Messrs. G. Huddleson, P. Coleman, and D. Gleason of the Aero Geo Astro Company, and to Messrs. A. Hamilton, J. Jekerley and L. Miner of the Collins Radio Company.

The author also wishes to express sincere thanks to Mrs. Agnes McLaughlin for typing this manuscript.

ABSTRACT

A radio receiver, capable of detecting VLF electromagnetic radiation generated in the magnetosphere, was included on the Injun III satellite. A loop antenna is used to detect the magnetic component of the VLF electromagnetic radiation at the satellite. A frequency spectrum analyzer on the satellite provides absolute measurements of the magnetic spectral density of the VLF radiation at six frequencies from 0.7 kc/s to 8.8 kc/s. The VLF signal, limited to a frequency band of approximately 0.5 - 7.0 kc/s is also telemetered to the ground by directly modulating the telemetry transmission at 136.860 Mc/s. In addition to the VLF measurements, simultaneous observations of auroral optical emissions and a wide variety of corpuscular particle measurements are obtained from the satellite.

On December 13, 1962, Injun III (1962 Beta Tau) was launched into an orbit having an inclination of 70.4°, an initial apogee altitude of about 2800 km., and a perigee altitude of 237 km. At the time of this writing (July 30, 1963) Injun III has transmitted approximately 600 hours of VLF data and is still transmitting useful information from most of the scientific experiments.

The results of the Injun III VLF experiment show that the intensity of VLF radiation observed in the ionosphere is in general much greater than on the ground. The maximum rms. amplitude, of the magnetic component in the 0.5 - 7.0 kc/s frequency band, which has been observed at the satellite is 8×10^{-2} gamma.

The amplitude of electromagnetic radiation from a VLF phenomenon known as chorus, considered as a function of the magnetic L coordinate of the satellite for local times between 0800 and 1300, shows a maximum at L = 5. The character of the amplitude variation with L was highly reproducible over the three day period studied.

Simultaneous occurrences of VLF electromagnetic emissions, auroral optical emissions, and particle precipitation into the atmosphere have been repeatedly observed. Two specific instances will be discussed.

TABLE OF CONTENTS

TABLE OF CONTENTS (Continued)

INTRODUCTION

The Very-Low-Frequency (VLF) range of the electromagnetic spectrum is considered to extend from approximately 1 kc/s to 30 kc/s. [Gallet, 1959a]. One may, in principle, use a suitable antenna and a very high gain audio amplifier with headphones to make direct (no frequency conversions) aural observations of a major portion of the VLF electromagnetic spectrum.

Several sources of naturally occurring VLF electromagnetic emissions have been of interest to geophysicists. Lightning provides one such naturally occurring source of VLF radiation. Electromagnetic impulses generated by lightning are called spherics. The propagation of spherics in the earth's magnetosphere was first studied by Storey. [Storey, 1963]. He found that spherics could be ducted along magnetic field lines from one hemisphere to another. The dispersive character of the medium in the magnetosphere was found to alter the frequency-time spectra of the original spheric. After one or more transversals through the magnetosphere[+], the original

---

+ In this note, "magnetosphere" is used to describe that portion of the outer atmosphere where the motion of a charged particle is dictated by the geomagnetic field.

spheric impulse is transformed into a wave packet called a whistler which, in the audio range, sounds like a whistle whose frequency monotonically decreases with time. Whistlers are commonly observed and have been conclusively shown to be initiated by lightning. [Morgan, 1958]. There are many observations of a wide variety of VLF "noises" whose detailed origin is unknown. [Gallet, 1959b],[Allcock, 1957]. Many of these VLF electromagnetic emissions exhibit distinctive frequency-time spectra which are crudely and qualitatively reproducible. For numerous classes of VLF electromagnetic emissions considerable evidence exists supporting the hypothesis that the electromagnetic waves are generated in the magnetosphere. [Gallet, 1959b], [Ellis, 1957], [Allcock, 1957].

Ground-based observations of those VLF phenomena which have their origin in the magnetosphere are subject to certain inescapable disadvantages. First, VLF waves propagating through the ionosphere are attenuated by approximately 35 db during the local day and approximately 10 db during the local night. [Leiphart, 1962]. The magnitude of the attenuation is found to be variable and relatively uncertain on any given occasion. Second,

waves generated in the magnetosphere may enter the ionosphere and travel considerable distances in the earth-ionosphere waveguide before they reach a ground station. [Martin, 1958]. The location of a VLF source in the magnetosphere is therefore difficult to determine. Third, man-made radiation often interferes with ground-based measurements of VLF phenomena. VLF observations below approximately 0.5 kc/s are greatly hindered by radiation from power systems. Fourth, in a study of the simultaneous occurrence of VLF emissions from the magnetosphere and intense electron precipitation into the atmosphere, the precipitation itself increases the ionospheric absorption above the observatory and hinders the observation of later VLF emissions. [Morozumi, 1962]. For all these reasons, and particularly because conversations with Dr. R. Gallet, Dr. P. Kellogg, and others had suggested that VLF phenomena might play a role in the acceleration of magnetospheric electrons, we decided to include a comprehensive VLF experiment on the satellite Injun III. The principal scientific aims of the satellite were to measure auroral optical emissions, the precipitated particles which cause them, and the VLF emissions which may accelerate the precipitated or trapped particles. [O'Brien, 1962a].

An external view of Injun III is shown in Fig. 1. The satellite shell is 24 inches in diameter and the total payload weight is about 114 lbs.

On December 13, 1962 Injun III (1962 Beta Tau) was launched into an orbit having an inclination of 70.4°, an initial apogee altitude of about 2800 km., and a perigee altitude of 237 km. At the time of this writing Injun III is still transmitting useful information from most of the scientific experiments.

A comprehensive understanding of VLF noise emissions from the magnetosphere will require an investigation of the following broad aspects of naturally occurring VLF electromagnetic emissions. First, the position, strength, and spatial extent of the magnetospheric VLF source must be determined for different classes of VLF emission phenomena. Second, the observable coupling of the VLF source with other geophysical phenomena must be studied. Third, the theoretical nature of these coupling mechanisms must be formulated. Fourth, experimental evidence must be presented which establishes the validity of these theoretical mechanisms. The purpose of this paper is to present evidence, obtained from satellite Injun III, relevant to the first two items in the preceding outline. First, the absolute amplitude of

VLF electromagnetic waves propagating to the satellite from a VLF emission known as chorus will be determined as a function of the spatial position of the satellite for a selected period. Second, measurements and observations regarding the association between aurorae, VLF electromagnetic emissions, and the precipitation of electrons into the atmosphere will be presented for two specific events.

Satellite-borne instruments which have preceeded Injun III in making measurements and observations of VLF radiation in the magnetosphere have been included on the Vanguard III [see Cain, 1961], Lofti I [see Leiphart, 1962], and Alouette [see Barrington, 1963] satellites.

VLF ELECTROMAGNETIC PHENOMENA, A SUMMARY

VLF electromagnetic phenomena are classified by the manner in which the spectral character of the emission changes with time. Often the spectral density of a signal is displayed at each frequency-time coordinate as darkness or intensity on a graph of frequency vs. time. A spectral analysis of a signal presented in this manner is called a frequency-time spectrogram or simply spectrogram. Spectrograms are commonly used in the interpretation of VLF phenomena.

Gallet has pointed out an important property of almost all known VLF phenomena: their reproducibility at different times and places. [Gallet, 1959b]. He has chosen to make the following systematic classification of VLF electromagnetic phenomena.

I. Whistlers - source, lightning.

II. VLF Emissions - not associated with lightning.

1. Continuous

2. Discrete

III. Interactions Between Whistlers and VLF Emissions.

Whistlers are VLF electromagnetic impulses generated by lightning which have had their frequency-time spectra

modified as the result of dispersive propagation over very long paths through the magnetosphere. A frequency-time spectrogram of a whistler usually shows a single tone or tones whose frequencies monotonically decrease with time. Helliwell has categorized whistlers into several types on the basis of their characteristic appearance on a frequency-time spectrogram. [Helliwell, 1959.] See Fig. 2 for an example of a frequency-time spectrogram of whistlers observed with Injun III. The darkened portion of the spectrogram indicates the more intense signal. Note the magnitude of the units on the frequency and time axes.

VLF emissions are taken to be all naturally occurring VLF phenomena whose direct source is not attributable to lightning impulses. VLF emissions have been classified as continuous or discrete. A continuous emission is characteristic of a steady state process. A continuous emission appears as a time stationary noise band on a spectrogram and is usually called hiss. A discrete emission is characterized by a distinctive appearance on a frequency-time spectrogram and represents a transient phenomenon. The class of discrete VLF emissions can be subdivided into a very extensive set of distinct,

recognizable, and reproducible VLF phenomena. The classes of discrete emissions are often named after their distinctive appearance on a frequency-time spectrogram. Examples are hooks, risers, pseudo whistlers, etc. [Jones, 1963]. The third class of VLF phenomena, interactions between whistlers and VLF emissions, concerns events where a whistler or spheric impulse serves to stimulate a VLF emission. On a frequency-time spectrogram this phenomenon appears as a whistler followed by a VLF emission. VLF emissions have been artificially stimulated from the magnetosphere, hence, the stimulating source is not limited to whistlers. [Helliwell, 1962a].

A brief summary of the present knowledge concerning two classes of VLF emission phenomena will now be presented. The two classes of VLF emissions to be discussed are "chorus" and "auroral hiss". These two phenomena will be the subject of primary interest in the results of the Injun III VLF experiment.

Chorus

Chorus has been described by Storey as a VLF emission consisting of a multitude of rising tones. He describes the audible chorus sounds from a VLF receiver

as sounding like a distant rookery. [Storey, 1953]. As seen on a frequency-time spectrogram chorus is a VLF emission consisting of a succession of short discrete emissions, usually rising tones, which often overlap in time. At middle latitudes the rising tones usually range from about 2 to 4 kc/s. [Allcock, 1957]. Chorus emissions extending from 0.5 kc/s to 15 kc/s have been observed. Emissions below 1.5 kc/s are common at higher latitudes [Ungstrup, 1963]. The period between successive discrete emissions in chorus may be as long as several seconds. Occasionally, when "bursts" of chorus activity occur, the short discrete emissions may arrive so rapidly that successive tones are indistinguishable. [Allcock, 1956]. See Fig. 3 for examples of frequency-time spectrograms of chorus observed with Injun III.

The origin of chorus emissions is not understood but it is often suggested that the electromagnetic emissions are generated in the ionosphere or magnetosphere by interactions involving electron bunches or electron streams moving with high velocity through the medium. [Gallet, 1959a], [Dowden, 1963].

It has been shown, on the basis of the occurrence frequency of the chorus phenomena as observed by ground

VLF stations, that chorus emissions most frequently occur in the morning. [Allcock, 1956], [Allcock, 1957]. The detailed character of the variation in chorus activity with local time differs from station to station. Pope has shown that the local time of maximum chorus activity moves to later hours at higher geomagnetic latitudes. [Pope, 1960]. The occurrence of chorus is also correlated with magnetic activity. [Allcock, 1957]. The correlation of chorus activity with magnetic activity is positive at middle latitudes and negative at high latitudes. [Ungstrup, 1963]. Allcock has concluded that the occurrence of chorus is more closely dependent on local magnetic disturbances than on large scale global magnetic disturbances. For middle latitudes, Helliwell concludes, on the basis of simultaneous observations of chorus at several ground stations, that the region of the lower ionosphere illuminated by the VLF electromagnetic wave from a discrete chorus emission is probably about 500 km. in diameter. [Helliwell,1962b], [Martin, 1956]. Observations in Antarctica, by Helliwell, indicate that at high latitudes the VLF emissions are highly localized, the region of the lower ionosphere illuminated by the VLF emission being perhaps a few tens

of kilometers in diameter. Since VLF emissions can propagate great distances in the earth-ionosphere waveguide, the exact determination of the spatial extent of chorus emissions using ground station measurements is difficult.

Auroral Hiss

The term "hiss" has been commonly used to describe VLF electromagnetic emissions whose frequency-time spectra appear as time-stationary noise bands. Hiss differs from chorus in that discrete emissions are not distinguishable in the emission spectra. The center frequency and band-width of hiss emissions varies from observation to observation and extends over a very wide range of frequencies and band widths. A class of hiss known as "auroral hiss" has been shown to be closely associated with the occurrence of aurorae. The center frequency of auroral hiss is usually about 8 kc/s and the band-width of the emission spectra is usually relatively wide, with frequency components often extending above 16 kc/s. [Martin, 1960].

Ellis has classified hiss on the basis of the observed frequency spectra of the emission and found that hiss emissions whose spectra extended from 4 to 8 kc/s

and 2 to 30 kc/s were clearly associated with local magnetic disturbances and auroral activity. [Ellis, 1959]. Martin and Helliwell, using observations in Antarctica, established a distinction between hiss occurring below 4 kc/s and "auroral" hiss occurring above 4 kc/s on the basis of their diurnal behavior. [Martin, 1960]. At Byrd Station in Antarctica, the diurnal variation of the average amplitude of hiss occurring above 4 kc/s shows two distinct maxima, each corresponding to periods of maximum auroral activity. The diurnal variation of hiss occurring below 4 kc/s, however, shows a single peak occurring in the local morning and resembles the diurnal variation of chorus at lower latitudes. Using statistical arguments a close association between the occurrence of hiss above 4 kc/s and the occurrence of aurorae was established. Morozumi, using his observations in Antarctica, found a close association between VLF hiss and auroral arcs and bands. [Morozumi, 1962]. Helliwell and Morozumi have noted that a VLF hiss emission is not always directly associated with the occurrence of an aurora. Occasionally VLF hiss emission is undetectable on the ground even in the presence of an intense and active aurora. This observation has been attributed to

the attenuation of the VLF hiss signal in the lower ionosphere because of enhanced ionization caused by the precipitated particles exciting the aurora. The intensity of the VLF hiss emission, generated in the upper ionosphere during an auroral optical emission, may not, therefore, be directly measurable from ground-based VLF observations.

THE INJUN III VLF EXPERIMENT

A block diagram of the Injun III VLF experiment is shown in Fig. 4. A loop antenna is used to detect the magnetic component of the electromagnetic wave in the frequency range of interest. The satellite is oriented by a large permanent magnet such that the geomagnetic field vector $\vec{B}$ is in the plane of the loop antenna. This orientation provides optimum coupling between the antenna and an electromagnetic wave propagating in the whistler (longitudinal extraordinary) mode. [Ratcliffe, 1959]. In this mode of propagation the wave is characterized as essentially a circularly polarized wave propagating along the geomagnetic field line. The plane of the loop and the satellite shell are separated by a distance of 15 cm. [See Fig. 1]. The surface of the satellite shell and the electrostatic shield wrapped around the loop antenna are coated with a dielectric material. It was experimentally verified by tests near the surface of the earth that the perturbation caused by the presence of the satellite shell was negligible. The nature of the perturbation caused by the satellite shell in an ionized medium (i.e., in orbit) is unknown. It is assumed in the following largely qualitative analyses

that any such effect is negligible.

The VLF antenna and preamplifier have been designed in such a manner that the signal from the preamplifier is representative of the magnetic component of the electromagnetic wave coupling the loop antenna (for a discussion of the antenna and the instrument calibration see the appendix.) The preamplifier signal is presented to a six channel frequency spectrum analyzer from which the absolute amplitude of the magnetic component of the wave can be determined at six frequencies, 0.7 kc/s, 2.7 kc/s, 4.3 kc/s, 5,5 kc/s, 7.0 kc/s and 8.8 kc/s, respectively. Each frequency channel samples a 50 c/s band of the frequency spectrum. The dynamic range of the spectrum analyzer is 40 db. The dynamic range may be shifted in two 20 db steps with an attenuator controlled by the satellite memory. Analog to digital converters in the satellite data system quantize the 40 db dynamic range into sixteen steps, each step 2.5 db wide. The output from a specific channel is processed by the satellite data system in such a manner that the satellite transmits the <u>minimum</u> amplitude occurring in the time interval since the previous sample was transmitted. The rate at which a given analyzer channel may be sampled is

controlled by the satellite memory. The maximum sampling rate is twelve samples per second. The sampling mode most commonly used in orbit is one sample every two seconds. Because the minimum amplitude occurring over an interval of time is sampled, the spectrum analyzer measurement gives the absolute amplitude distribution of the slowly varying background noise spectrum and ignores the transient noise burst whose time constants are much shorter (less than 0.1 seconds) than the sample interval. The spectrum analyzer measurement does not, therefore, respond to lightning impulses.

The preamplifier signal, limited to a frequency band of approximately 0.5 - 7.0 kc/s and normalized to a constant amplitude by an automatic gain control (A.G.C.) circuit, is used to directly modulate the telemetry transmission at 136.860 Mc/s. The VLF signals thus telemetered to the ground can be analyzed with high time resolution spectrum analysis equipment. The automatic gain control feedback voltage is used as a measure of the rms wide-band magnetic field strength in the frequency band 0.5 - 7.0 kc/s. The frequency response of the wide-band VLF system, with the gain of the A.G.C. circuit held constant, is shown in Fig. 5. The response time constant

of the automatic gain control feedback loop is approximately 0.2 seconds.

The following three measurements are, therefore, obtained from the Injun III VLF experiment. First, the absolute amplitude of the magnetic component of the VLF wave is measured at six frequencies. Second, the wide-band magnetic field strength in the frequency band 0.5 - 7.0 kc/s is measured. Third, high time resolution frequency time spectra can be obtained from the wide-band VLF signal which is telemetered to the ground. These measurements are complementary in the following sense. High time resolution frequency-time spectra cannot be obtained from the satellite borne spectrum analyzer because of the low sampling rate. The wide-band VLF signal telemetered to the ground may, however, be processed with high time resolution analyzers such as the Rayspan spectrum analyzer. VLF spectral characteristics resembling time-stationary white noise may be indistinguishable from communication noise to the observer, using the wide-band VLF signal telemetered to the ground. Slowly varying spectra of this type are, however, easily analyzed using the satellite borne spectrum analyzer.

The noise level of the receiver stated in terms of an equivalent magnetic spectral density applied to the antenna is approximately 5.0×10^{-11} $(\text{gamma})^2(\text{c/s})^{-1}$ (See the Appendix.) We shall now compare this equivalent receiver noise level with VLF flux densities observed on the ground from magnetospheric VLF emissions. The lower atmosphere can be considered as a nonconducting medium having an index of refraction of unity. For such a medium the equivalent receiver noise level stated above corresponds to a VLF spectral power density of approximately 1.2×10^{-14} watts $(\text{m})^{-2}(\text{c/s})^{-1}$. Ellis quotes VLF flux densities from magnetospheric VLF emissions, observed by him, on the ground, ranging from 6×10^{-19} to 10^{-16} watts $(\text{m})^{-2}(\text{c/s})^{-1}$. [Ellis, 1959]. It appears, therefore, that the sensitivity of the Injun III VLF receiver is not in general adequate for detecting magnetospheric VLF emissions from the ground.

Considering only magnetospheric VLF sources it was anticipated prior to launch that the following factors may operate to increase the intensity of the magnetic component of the VLF wave at the satellite, relative to a ground-based observation. First, in a plasma, for a given wave power, more of the energy is stored in the

magnetic component. Second, the VLF electromagnetic wave generated in the magnetosphere and reaching the satellite will not be attenuated by the ionosphere. Third, if the VLF electromagnetic waves are radiated essentially isotropically from the source region, very large VLF power fluxes may be observed when the satellite is in close proximity to the source. Fourth, if magnetospheric ducting of VLF waves occurs, the VLF power density in the duct at large distances from the source may be comparable to the power density in the source region. Thus, very intense VLF power fluxes may be observed when the satellite is in a duct. [Smith, 1960]. At the time that the Injun III experiment was designed the only direct observations of naturally occurring VLF signals above the ionosphere came from whistler observations with Vanguard III. [Cain, 1961]. Estimates of Whistler amplitudes obtained from these observations indicated that the magnetic component of whistlers propagating in the magnetosphere occasionally exceeds one gamma. This amplitude is relatively large compared to ground-based observations and encouraged the view that the

Injun III VLF experiment had sufficient sensitivity to make meaningful measurements in the magnetosphere. In fact, as will be seen, the actual sensitivity is quite adequate in flight.

MEASUREMENTS AND PARAMETERS USED IN THE VLF ANALYSIS

The geophysical measurements available from the Injun III experiment involve three types of instruments. First, the VLF experiment allows the identification of the spectral class to which a VLF emission belongs and it allows a measurement of the absolute amplitude spectrum of electromagnetic waves which have propagated to the satellite from the source of the VLF emission. Second, the intensity of auroral optical emissions at 5577$\mathring{A}$ and 3914$\mathring{A}$ can be measured by two photometers which, in general, view aurorae near the base of the field line passing through the satellite. The region of the atmosphere viewed by each photometer is determined by the satellite altitude and orientation. The field of view of each photometer is a cone (4 degree half angle) whose axis is aligned parallel to the geomagnetic field $\vec{B}$ vector by the satellite orientation magnet. Deviations from alignment with the geomagnetic field are usually less than 5 degrees and the deviation may be determined using the satellite magnetometer measurements. Third, a wide variety of corpuscular radiation measurements are performed on Injun III. The corpuscular radiation data which are significant in this preliminary report were

obtained from detector number 5. [O'Brien, 1962a]. Detector 5 is a type 213 geiger tube and is sensitive to electrons whose energy exceeds approximately 40 kev. and protons whose energy exceeds approximately 500 kev. The field of view of this detector is a cone (43 degrees half angle) whose axis is parallel to the geomagnetic field $\vec{B}$ vector and is directed upward in the northern hemisphere. Detector 5 is, therefore, sensitive to sufficiently energetic particles moving downwards in the northern hemisphere and having pitch angles less than 43 degrees. For appropriate altitudes this detector provides a measure of the intensity of precipitated electrons having energies exceeding 40 kev. [See O'Brien, J. Geophysical Research, September, 1962b, for a discussion of precipitated electrons with energy greater than 40 kev.] With these three instruments, Injun III may make simultaneous observations of auroral optical emissions, particle precipitation into the atmosphere, and VLF electromagnetic emissions.

The spectral class to which a VLF emission, observed at the satellite, belongs is determined primarily from frequency-time spectrograms of the wide-band-VLF signal telemetered to the ground. Two types of spectrum analyzers have been used in this analysis to generate frequency-time spectrograms. The two analyzers differ in that the first,

the comb-filter type analyzer, provides time resolution of approximately 10 milliseconds. For the second type, the sweep-filter analyzer, the time resolution is approximately 2 seconds. Spectrograms are usually presented on photographic film or some type of photosensitized paper. Examples of wide-band VLF signals telemetered from the satellite to the ground and analyzed with low and high resolution analyzers are shown in Fig. 6 and Fig. 3 respectively. The darkened portion of a spectrogram indicates the stronger signal. Corresponding points on the low and high resolution spectrograms can be found at L = 4, 1453 UT on the December 19 data. The analyzers used for low- and high-time resolution spectrograms in this analysis are, respectively, the Proboscope Model SS-100 and the Raytheon Rayspan analyzer. High resolution spectrograms provide much greater spectral detail than the low resolution spectrograms, but because of the long, unweildy films involved the analysis of temporal changes on the order of several minutes is very tedious. Many of the commonly occurring VLF emissions can be identified with low resolution spectrograms. For these reasons low resolution spectrograms have been extensively used in this analysis.

In the low time resolution sweep type analyzer, the frequency-time spectrogram is derived from the output amplitude of a single filter whose center frequency periodically scans the frequency spectrum of interest. The scanning process is usually accomplished by heterodyneing the signal to the center frequency of the filter and sweeping the heterodyne frequency. The time resolution possible with a sweep-filter analyzer is equal to the scan period (2 seconds in our case). A spectrogram display is obtained by intensity-modulating an oscilloscope beam whose horizontal position on the screen is determined by the center frequency of the filter. A strip film camera slowly moves a film along the vertical axis to generate the temporal scale on the film.

The second type of spectrum analyzer, known as the comb-filter analyzer, provides a considerable improvement in the time resolution of spectrograms. In the comb-filter analyzer, the signal to be analyzed is simultaneously applied to a large set of filters. The center frequencies of the filters are staggered so that frequencies throughout the frequency band of interest are sampled. The spectral density of the applied signal at the center

frequency of a specific filter is obtained by measuring the output amplitude of that filter. By sequentially sampling the filter outputs the temporal changes in the frequency spectrum of the original signal may be displayed. As the sampling process may be in principle arbitrarily fast, the time resolution of the analyzer is limited only by the band widths of the individual filters. The envelope response time constant of a narrow band filter is given by $\tau = 1/\pi B$, B is the filter band width. [Martin, 1951]. It is apparent from this expression that the frequency and temporal resolution of an analyzer is limited by filter considerations. Because a comb-filter type analyzer has many filters, the information band width is much larger than with a sweep type analyzer. Thus, the time resolution is much better for the comb-filter type analyzer. The Rayspan comb-filter analyzer, used to process data in this analysis, has 420 filters and will analyze a frequency band from 100 cps to 10 kc. The spectrogram is generated using a system very similar to the oscilloscope and strip film camera used with the low resolution analyzer.

Most of the VLF emissions observed at the satellite can be identified as a member of various classes of VLF

phenomena on the basis of their frequency-time spectrograms. Our nomenclature regarding the various classes of VLF phenomena will follow as closely as possible the presently accepted terminology. Two classes of VLF phenomena have been selected for study with the Injun III VLF experiment. The selected classes are "chorus" and "auroral hiss".

The presence of a chorus emission can be identified from the Injun III VLF measurements using the following considerations. First, using the wide-band VLF signal telemetered to the ground, the spectral character associated with a chorus emission can usually be identified with high time resolution spectrograms, low time resolution spectrograms, or aural monitoring. Second, the distinct rising tones characteristic of chorus emission tend to start and terminate abruptly. When a chorus emission is being detected by the satellite VLF receiver considerable fluctuations usually exist in the wide-band signal strength measurement. Low time resolution spectrograms usually show chorus as irregular blotches extending over the emission band width. See Fig. 6 and Fig. 7 as examples of low resolution spectrograms of chorus. If the low resolution spectrogram shows a spectrum characteristic of chorus and the wide-band signal strength is

fluctuating rapidly, it is considered that there is a good indication of a chorus emission. Positive identification must be made by aural monitoring or high time resolution spectrograms.

The presence of an auroral hiss emission can be best identified from the Injun III VLF measurements by using the satellite-borne spectrum analyzer data. The magnetic spectral density of the VLF hiss radiation at the satellite is measured for each of the six analyzer frequencies. An auroral hiss emission, being a wide-band noise signal, appears as a simultaneous response from all the VLF spectrum analyzer channels above approximately 4 kc/s. The wide-band signal strength measurement can be used to complement the spectrum analyzer measurements. Wide-band hiss cannot always be positively identified using the wide-band VLF signal telemetered to the ground because the VLF signal may not be distinguishable from communication noise.

The geophysical observations performed at the satellite may be related to the satellite coordinates in space and time and to geophysical phenomena observed by other means. We shall now consider the possible satellite coordinates in space and time and their significance

relative to an observation of a VLF electromagnetic wave at the satellite. It must be recognized that the VLF measurements of spectra and amplitude involve the observation of a wave which has propagated from the VLF source region to the satellite. Inferences regarding the nature and spatial distribution of the VLF source from measurements at the satellite require knowledge of the viewing region of the VLF antenna into the ionosphere and magnetosphere. Knowledge of the viewing region of the VLF antenna will be understood to mean a description of the propagation conditions from the source to the satellite together with the directional properties of the antenna, this description to consider all source positions. The nature of this viewing region has to our knowledge never been subjected to experimental, quantitative measurements using a magnetospheric VLF source. On the basis of whistler observations, it is generally thought that VLF electromagnetic waves propagating in the magnetosphere are guided to some degree along the geomagnetic field line. [Storey, 1953]. Storey was able to show that in a medium containing only electrons and a uniform magnetic field the maximum angle between the direction of effective energy propagation (ray direction) and the magnetic

field does not exceed about 20 degrees. If heavy ions are considered in the analysis of electromagnetic wave propagation in a magnetoionic medium, it is found that propagation can occur for any angle between the ray direction and the magnetic field. [Hines, 1957]. The extent to which propagation can occur at large angles to the magnetic field increases with increasingly heavy ion density and lower frequency. Smith and others have suggested that VLF electromagnetic energy is guided along geomagnetic field lines by field-aligned ionization in the magnetosphere. [Smith, 1961].

On the basis of the above discussion of the propagation of VLF electromagnetic waves in the magnetosphere a very general model has been hypothesized to aid in the interpretation of the Injun III VLF data. The model illustrated in Fig. 8 has been constructed using the thought that there exists some surface having symmetry about a geomagnetic field line inside which VLF electromagnetic waves radiated from a source would freely propagate to the satellite. Outside of this surface, propagation of VLF waves to the satellite would be strongly attenuated. Three regions of propagation are defined in this model. In region I, VLF waves propagate in the earth-ionosphere waveguide. Lightning is considered the only significant

source of VLF radiation occurring in region I. Region II is the region between the satellite and lower boundary of the ionosphere. VLF electromagnetic waves radiated from a source located in region II propagate to the satellite in the whistler (longitudinal extraordinary) mode. Lightning impulses generated in region I and coupled into region II are attenuated in traversing the ionosphere. Region III is considered to extend outward into the magnetosphere above the satellite as illustrated in Fig. 8.

The validity of the model presented here rests largely on the extent to which heavy ions allow propagation to occur at large angles to the geomagnetic field lines. Hines has indicated that, for the case of a single type of heavy ion, the maximum angular frequency ω at which the presence of heavy ions is significant is given by $\omega = eB/(M_e M_i)^{1/2}$, $\vec{B}$ the magnetic field, M_e the electronic mass, M_i the ion mass. [Hines, 1957]. For a geocentric distance of approximately two earth radii, considering hydrogen ions and electrons as the constituents, the transition frequency is approximately 4 kc/s. It appears that the validity of the model presented here will depend strongly on the altitude of the

satellite and the frequency under consideration.

We choose to investigate the nature and amplitude of VLF electromagnetic emission as a function of the spatial coordinates of the satellite and to consider as a second step the analysis of the source regions viewed by the antenna for these coordinates. The McIlwain L shell parameter commonly used in the analysis of trapped corpuscular radiation is implicitly contained as a parameter in the model viewing region of the VLF antenna. Because we seek relationships between VLF and corpuscular radiation the L shell parameter may be expected to serve as a useful coordinate in the analysis of the satellite observations of VLF phenomena. [For a discussion of the L shell parameter see C. E. McIlwain, 1961]. Because the transition frequency at which heavy ion effects become significant varies with $\vec{B}$, the geocentric distance or satellite altitude must be considered a relevant coordinate in the analysis. Ground-based VLF observations have established a variation in the occurrence rates of various VLF phenomena with local time. [Allcock, 1957]. Local time at the satellite would appear, therefore, to be a significant parameter in the analysis. The VLF observations performed with Injun III may, therefore, be

considered as functions of the L shell parameter, local time at the satellite, and the altitude of the satellite.

RESULTS OF THE INJUN III VLF EXPERIMENT

A. VLF Phenomena Detectable with Injun III

We shall agree to recognize the presence of a VLF electromagnetic phenomena observed at the satellite, when either the quantized decimal readout of the wide-band signal strength measurement is greater than 3 or when a VLF spectrum characteristic of the phenomena can be recognized from the wide-band VLF signal telemetered to the ground. The threshold which must be exceeded to give a signal strength measurement exceeding 3 is 10^{-3} gamma for the wide-band signal strength measurement. (See Appendix for a discussion of the calibration.) The threshold for recognition of a VLF phenomenon using the telemetered wide-band VLF signal is highly dependent on the spectral character of the phenomenon and is always less than 10^{-3} gamma when the communication signal to noise ratio exceeds 20 db, as it does when useful digital data are accepted by the computer which does the data reduction. VLF phenomena of a discrete transient nature may be recognized with the telemetered wide-band signal but may not give a detectable wide-band signal strength measurement because of the slow sampling rate for this measurement (one sample every 4 seconds). It is possible,

therefore, that a strong whistler may be recognized aurally with the telemetered wide-band VLF signal, but the wide-band signal strength may not be sampled at the proper instant to determine the amplitude of the whistler.

Noise impulses showing little dispersion are commonly observed at the satellite via the wide-band VLF signal telemetered to the ground. These impulses are presumed to be spherics, which have propagated a relatively short distance from region I, through region II, and to the satellite. Barrington calls noise impulses of this type, observed in the ionosphere, short fractional-hop whistlers. [Barrington, 1963]. Long fractional-hop whistlers are spheric impulses which have crossed the magnetic equator in propagating through the magnetosphere. Long fractional-hop whistlers are also commonly observed at the satellite.

No quantitative studies have been attempted concerning the propagation of whistlers in the magnetosphere. Some qualitative statements are, however, in order. Spheric impulses could always be heard during tests on the ground using the satellite VLF receiver and antenna. However, for the total observation time on the ground,

estimated to be 15 hours extending over two months, only three whistlers and no VLF emissions of any type were identified. After the satellite was launched the same receiver and antenna has detected many long fractional-hop whistlers in the ionosphere. In some instances as many as 20 long hop whistlers per minute have been heard. It has also been observed that the background spheric (short fractional-hop whistlers) noise level in the ionosphere is much lower than on the ground. Instances have been found, for periods up to 17 minutes, where no VLF spheric impulses were detectable at the satellite. A steady background of spheric impulses could always be heard with the satellite receiver and antenna on the ground. These observations serve to illustrate the large ionospheric attenuation occurring when VLF electromagnetic waves propagate from region I to region II (see Fig. 8).

It has been suggested that the motion of the satellite through the upper ionospheric medium may generate local electromagnetic fluctuations or oscillations via interactions with the magnetic field of the orientation magnet or ion flow around the satellite shell. If such oscillations are associated with the motion of Injun III

through the ionosphere, they may be detectable with the VLF receiver and may be erroneously interpreted as naturally occurring VLF emissions. The following observation is used to support the hypothesis that the motion of the Injun III satellite through the ionosphere does not generate VLF electromagnetic emissions of sufficient amplitude to be detectable with the VLF receiver. The spectral character of discrete VLF emissions observed at the satellite is not unlike those commonly observed with ground-based VLF receivers. This would argue that discrete emissions observed at the satellite are not the direct result of the motion or presence of the satellite in the ionosphere. It must be admitted, however, that the above fact does not deny the possibility that the motion or presence of the satellite may trigger or enhance some naturally occurring VLF emission process. Lacking further evidence concerning the possibility of self-induced VLF emissions we shall be forced to assume in the following analysis that the presence of the satellite in the ionosphere represents a negligible perturbation of naturally occurring VLF emission processes.

A relatively rare phenomenon, which has been observed with the Injun III VLF receiver on several occasions, is the excitation of VLF emissions by spheric impulses, which have propagated to the satellite. The emissions, which always start immediately after the triggering whistler, are often of an exceedingly complex frequency-time structure consisting of several tones of changing frequency. Enhancement of whistler triggered emissions appears to occur during certain times. Passes have been observed where 40 percent of all spheric impulses observed at the satellite were followed by emissions, even for relatively weak impulses. Other passes occur where no triggered emissions occur, even when very strong spheric impulses are observed. No detailed quantitative studies have been attempted concerning the propagation of spheric impulses in the magnetosphere or their interaction with the magnetospheric medium.

The Injun III satellite electronics system and VLF experiment were carefully designed so that no electromagnetic radiation from the satellite electrical system would be detectable with the VLF experiment. Tests prior to the launching of the satellite indicated that these objectives had been attained. It was established, for

instance, that the response of each detector to its appropriate stimulus did not in any way interact with the VLF measurements. Prior to April 5, 1963, no evidence had been found from the data obtained from the satellite in flight which suggested that any form of radiation originating from the satellite was detectable with the VLF experiment. Starting April 5, 1963, a periodic clicking with a variable period, usually about 2 seconds, has been occasionally heard from the wide-band signal telemetered to the ground. This signal is presumed to originate from within the satellite electronics system. It has been established that this interference source, which is of a transient nature, is not of sufficient amplitude to be measurable with either the wide-band signal strength or the spectrum analyzer measurements. All data presented in this analysis was obtained before April 5, 1963. No VLF signal radiated from a man-made source has ever been identified from observations in the ionosphere with the Injun III VLF experiment.

The remainder of this paper will consider only VLF emission phenomena as defined by Gallet and discussed earlier. Of all the observations telemetered by the

satellite during January 1963, VLF electromagnetic waves, associated with VLF emission phenomena, were present at the satellite with sufficient intensity to exceed the detectability threshold of the wide-band signal strength measurement for 24 percent of the total telemetering time. Satellite data received at high geomagnetic latitude stations such as College, Alaska show measurable VLF emissions for as much as 60 percent of the observation time during January.

The maximum rms amplitude VLF radiation observed with the wide-band signal strength measurement during January, 1963 was 5×10^{-2} gamma. This observation was made at 1554 UT, January 30, 1963. The L coordinate of the satellite was L = 6 and the satellite altitude was 320 km. In this instance the VLF phenomenon occurring was determined to be a wide-band hiss emission of the type usually associated with aurorae. The magnetic spectral density of the hiss radiation, calculated on the basis of a 7.0 kc/s receiver band-width, is 3.6×10^{-7} $(\text{gamma})^2(\text{c/s})^{-1}$. Ellis states 10^{-16} watts $(\text{m})^2(\text{c/s})^{-1}$ as the maximum spectral power density of auroral hiss observed by him on the ground. [Ellis, 1959]. This spectral power density corresponds to a magnetic spectral

density of 4.3×10^{-13} (gamma)^2(c/s)$^{-1}$. The maximum magnetic spectral density of auroral hiss observed by Injun III in the ionosphere, therefore, exceeds the maximum magnetic spectral density of auroral hiss observed on the ground (as observed by Ellis during previous studies) by a factor of 10^6. These observations serve to illustrate the intensity of VLF electromagnetic radiation observed with Injun III.

Hiss having frequencies less than 1 kc/s and chorus are the electromagnetic emissions most commonly observed at the satellite. Hiss in this frequency range will be called extra low frequency (ELF) hiss. In many cases, ELF hiss observed at the satellite having frequency components as low as 200 c/s, can be recognized with frequency-time spectrograms obtained from the wide-band VLF signal telemetered to the ground. At 200 cps it is seen from Fig. 5 that the frequency response of the wide-band VLF receiver is down 22 db from the mid-band value. The ELF hiss is often characterized by a sharply defined upper frequency limit. The absolute spectral densities of frequencies less than 1 kc/s are difficult to analyze because of the nonuniform frequency response of the VLF receiver-antenna system at these

frequencies. No comprehensive quantitative study has been attempted concerning ELF hiss emissions observed at the satellite. Because man-made radiation makes ground-based observations at ELF frequencies difficult, the rather common observations of electromagnetic emissions in the ELF region with Injun III are considered of potential importance in the study of magnetospheric phenomena.

B. VLF Chorus Emissions Observed with Injun III

We shall now investigate the nature and amplitude of the VLF electromagnetic radiation from chorus emissions as a function of the spatial coordinates of the satellite. As discussed earlier an appropriate set of satellite coordinates for the investigation of VLF phenomena would be the local time at the satellite, the altitude of the satellite, and the L shell parameter associated with the geomagnetic field line passing through the satellite. The periodic nature of the satellite trajectories through these coordinates allows the repeated observation of VLF activity in a selected region of this coordinate space. A general observation from Injun III has been that chorus emissions are observed consistently from pass to pass over some limited portion of the orbit.

Because numerous other magnetospheric phenomena are strongly dependent upon the L shell parameter it was decided that the amplitude of VLF chorus radiation at the satellite would be investigated as a function of this parameter. To conveniently study the L dependence of the amplitude of chorus radiation it would be desirable to hold the local time and altitude coordinates constant while varying L. As the local time and altitude coordinates cannot be held constant because of the orbit, data must be selected which minimizes the variations in these coordinates or it must be demonstrated that the amplitude measurement is not a significant function of these coordinates.

Variations with local time can be minimized by selecting only passes for which the L coordinate increases or decreases very rapidly with local time. A series of satellite trajectories in L and local time coordinates is shown in Fig. 9. Using the criterion that acceptable passes cover the range of L values from 2 to 10 for local times between 0800 and 1300, six passes were selected for analysis. The revolution numbers associated with these passes are 69, 70, 71, 80, 93, and 105. During this period the satellite was not

aligned with the geomagnetic $\vec{B}$ field because oscillations associated with the injection into orbit had not yet damped. No attempt will be made to correct for the variable antenna orientation. The average planetary geomagnetic K_p index for the three day period being considered was approximately 5.

Low resolution spectrograms typical of the VLF emissions observed at the satellite during these passes are shown in Fig. 6 and Fig. 7. Using high resolution spectrograms it was established that the most intense VLF emission occurring during each of the selected passes was chorus. Chorus appears on the low resolution spectrograms as irregular blotches from 1 to 4 kc/s and predominantly for L values between 2 and 6. The extent to which VLF chorus emissions were detectable with the wide-band VLF signal strength measurement and identifiable with high resolution spectrograms is shown symbolically in Fig. 9. Since chorus was the most intense VLF emission occurring during the selected passes, the wide-band VLF magnetic field strength measurement may be taken as a measure of the rms amplitude of the magnetic component of the VLF chorus radiation coupling the loop antenna. Three difficulties arise if we attempt to calculate an

absolute VLF wave power density from these measurements. First, the index of refraction of the medium is not accurately known. Second, the perturbation caused by the presence of the satellite shell is not known. Third, the angle between ray direction of the VLF wave and the normal to the plane of the loop antenna is not known.

The result of an analysis of the dependence of the wide-band signal strength measurement on the L shell coordinate of the satellite for the selected passes is shown in Fig. 10. For each pass an average rms wide-band magnetic field strength (in gammas) was determined for each integral L value by calculating the average value of the wide-band magnetic field strength measurements between L-1/2 and L+1/2. The altitude and local time coordinates of the satellite were calculated for each integral value of L. The following items have been tabulated for each integral value of L and for each of the selected passes: (A) the rms wide-band magnetic field strength measurements averaged from L-1/2 to L+1/2, (B) the altitude of the satellite, and (C) the local time coordinate of the satellite. The six selected passes provide approximately 1,200 data points distributed over L values from 2 to 14. The results

shown in Fig. 10 were obtained by averaging item A over the six selected passes for each integral value of L. The standard deviation of this average is shown as σ. The dependence of the average rms wide-band signal strength, tabulated as item (A), upon the satellite altitude and local time coordinates are shown as scatter diagrams in Fig. 11 and Fig. 12 respectively. For the six selected passes, the spatial dependence of the amplitude of VLF chorus radiation observed at the satellite is, therefore, presented collectively by the result shown in Figs. 10, 11 and 12.

The results just presented will be used to support the following hypothesis. Of the three coordinates considered and their respective ranges, the amplitude of VLF chorus radiation observed at the satellite for the six selected passes depends primarily on the L shell coordinate of the satellite and is as shown in Fig. 10. This hypothesis is supported as follows. A systematic variation of VLF wide-band signal strength with L is observed. It has been shown that the VLF emission giving rise to the measurements is chorus. The satellite orbit, however, couples variations in the satellite L coordinate with variations in the satellite altitude.

It may be the case that the observed amplitude variation with L is actually the result of a systematic variation in satellite altitude. The scatter diagram Fig. 11, however, does not show a systematic dependence of the wide-band signal strength on altitude. We conclude, therefore, that the observed variation with L is essentially independent of the satellite altitude. No strong systematic variation in the wide-band signal strength with local time is apparent in the scatter diagram Fig. 12. This result supports the validity of the original selection criterion, which was intended to decrease the influence of chorus amplitude variations with local time.

The amplitude of the VLF radiation, from the source of the chorus emission, shows an L dependence having a well defined maximum at L = 5. The relatively small standard deviation of the measurements indicates that the amplitude of the VLF chorus radiation in successive passes was highly reproducible at each L value during the three day period studied. The L parameter, as well as being a position coordinate for the satellite, was considered earlier in the discussion of the viewing region of the VLF antenna. The L parameter was used to define the region of the magnetosphere viewed by the VLF antenna.

If the model viewing region of the VLF antenna hypothesized in Fig. 8 is accepted, the observed dependence of the amplitude of chorus radiation on L strongly suggest that the source of the discrete VLF chorus emissions is located somewhere in the vicinity of the L = 5 geomagnetic shell. These observations are for a specific three day period and do not represent a general result applicable to all chorus emissions.

The spectral character of VLF chorus emissions has been compared at specific values of L for each of the selected passes. High time resolution spectrograms of VLF chorus emissions observed at the satellite for L = 4 are shown in Fig. 3 for four of the six selected passes. The universal time for each of these observations is noted. We shall consider the maximum and minimum frequency occurring in the emission spectra as characterizing the chorus emission. It can be seen from Fig. 3 that the spectral character of the VLF chorus emissions is not necessarily the same for observations in the same region of space (same L values, local time differing by less than 2.5 hours, and satellite altitudes differing by less than 400 km.) at times differing by one revolution period, or about two hours. It appears, therefore, that the spectral nature of VLF radiation

from chorus emission observed at the same region in space can change markedly in times less than two hours.

Using high resolution spectrograms of VLF chorus emissions detected with Injun III, instances can be found in which the chorus emission occurred over a narrow band of frequencies. This banded type of chorus emission can be characterized by a fairly well defined center frequency. In several instances it has been observed that the center frequency of the emission is remarkably independent of L, as though the VLF radiation from the same source region were being viewed over a range of L values. An example of a banded chorus emission having a very similar center frequency at L = 2 and L = 5 is shown in Fig. 13. The time difference between these two observations is approximately 7 minutes.

C. Auroral Hiss Emissions Observed With Injun III

We shall now present two observations obtained from Injun III, which illustrate the simultaneous occurrence of VLF hiss, auroral optical emissions, and particle precipitation into the atmosphere. The observations presented were obtained with Injun III from 0949 to 0954 UT, February 28, 1963, and from 0720 to 0725 UT, March 3, 1963.

These observations will be called the February 28 and March 3 events respectively. The following items are characteristic of both events. The observations were made during local night conditions. The moon was not visible from the satellite. The range of satellite altitudes involved during the periods of enhanced activity was between 250 and 350 km. The maximum error occurring in the magnetic alignment of the photometer viewing axis, relative to the geomagnetic $\vec{B}$ vector, was 4 degrees.

The alignment of the satellite, relative to the geomagnetic field to within the error stated, means that the following geometric considerations are known to apply to the February 28 and March 3 events. First, the photometers which view downward in the northern hemisphere are aligned to view optical emissions along the field line passing through the satellite. The alignment error of the photometer, always being less than the half angle of the photometer viewing cone, will be ignored in this analysis. Second, non-penetrating particles detected by detector number 5 are known to be moving downwards with pitch angles less than approximately 43 degrees. At the altitude that these observations were made, particles moving downwards with pitch angles less than 43 degrees will plunge into the atmosphere. Detector

number 5 may, therefore, be used as a measure of the particle flux precipitating into the same general region of the atmosphere viewed by the photometer. Third, the plane of the VLF loop antenna is known to be oriented such that the geomagnetic $\vec{B}$ vector is approximately parallel with the plane of the antenna. The VLF experiment provides, therefore, a measurement of the amplitude of the VLF magnetic component perpendicular to the geomagnetic B field. Interpretations of the VLF measurement, in terms of absolute quantities associated with the VLF electromagnetic field in the medium, must consider the difficulties previously mentioned concerning the unknown ray direction and the perturbation caused by the presence of the satellite shell.

The response of the VLF experiment, the 3914 $\mathring{A}$ auroral photometer viewing downward in the northern hemisphere, and detector 5 are shown for the February 28 and March 3 events in Fig. 14 and Fig. 15 respectively. The following four VLF measurements are shown as a function of time for each event: the wide-band VLF signal strength, and the magnetic spectral density of the VLF signal at 2.7 kc/s, 5.5 kc.s, and 8.8 kc/s. The absolute VLF magnetic spectral density measurements were obtained from the satellite-borne six channel spectrum analyzer and

are thought to be accurate to within 2.5 db. [See Appendix for a discussion of the calibration.] The sampling rate used in these observations was one sample every 2 seconds for the spectral density measurements and one sample every four seconds for the wide-band VLF signal strength measurement.

The relative intensity of the optical emissions viewed by the satellite at 3914 Å for the events being considered is shown in Fig. 14 and 15. It is thought that these emissions were of an auroral origin. Since the observations were made during the local night with the moon not visible from the satellite, the conditions required to view an aurora from the satellite were favorable. Optical emissions from lightning and cities provide other possible sources. The close association between the occurrence of optical emissions, particle precipitation, and VLF emissions observed during these events strongly suggests that the optical emissions viewed by the satellite photometer at 3914 Å were of an auroral origin. The photometer measurement has been corrected for the nonlinear instrument response to give the relative intensities plotted. The relative intensities at any given time in either event may be considered accurate

to within plus or minus 10 percent for values below 4×10^3 on the arbitrary intensity scale. Above 4×10^3 on the arbitrary intensity scale, relative intensities may be considered accurate to within a factor of 1.5. [H. Taylor, private communication]. Absolute intensities have not been explicitly shown for the 3914 Å photometer measurement because of a possible gain shift relative to the preflight calibrations. In flight calibrations are presently being attempted as a check on the preflight calibrations. The best present estimates of the peak absolute optical emission R_m occurring during the February 28 and March 3 observations are 1.6 kilorayleighs and 11 kilorayleighs, respectively. These estimates are considered accurate to within a factor of three. [H. Taylor, private communication]. Because of a possible uncertainty in the photometer calibration, we shall emphasize the relative temporal response of this measurement rather than absolute intensities. The photometer sampling rate used during these observations was approximately one sample every 2 seconds. Ground-based observations of the auroral optical emissions occurring in the regions viewed by the satellite photometers have not been considered in

the analysis of the two events being presented. It is, therefore, not possible to resolve variations in the optical emissions viewed in the temporal scale associated with the satellite's motion through space and time (8.2 km/s for these events) into spatial and temporal variations associated with the aurora.

The particle flux detected by detector 5 during the February 28 and March 3 events is shown in Fig. 14 and Fig. 15. The shaded area in Fig. 14 indicates a region of uncertainty in the true counting rate. For apparent counting rates less than 10^3 counts per second no corrections for the dead time of the instrument are required. Above an apparent counting rate of 10^3 counts per second some uncertainty exists concerning the correction required to obtain the true rate. The apparent counting rate of detector 5 has exceeded the maximum rate possible in the preflight calibrations by a factor of about 1.6. It seems plausible, considering the nature of the discrepancy, to assume that the true rate is bounded by the apparent rate and the rate calculated from the preflight calibration of the true vs. apparent counting rates. On the basis of this assumption the boundary of the region of uncertainty in Fig. 14 was established. During the February 28 observations the

peak rate does not exceed 10^3 counts per second; hence, the counting rate plotted in Fig. 15 is identical with the apparent rate. The directional flux intensities plotted in Fig. 14 and Fig. 15 have an additional uncertainty of $\pm$ 30 percent because of uncertainties in the geometric factor of this detector. [L. A. Frank, J. D. Craven, Note on the Characteristics of the G.M. Detectors on Injun III, SUI Memo, March 11, 1963]. The particle flux observed with detector 5 during the events being considered is known to be electrons on the basis of a null response from a proton sensitive p-n junction detector viewing in the same direction, and sensitive to a similar range of proton energies, as detector 5. The sampling rate for detector 5 during the observations being considered was 4 samples per second. Because the other detector responses which are being presented in the February 28 and March 3 events are being sampled at a much slower rate there appeared to be no reason to display the precipitated particle flux at 4 samples per second. For this reason the particle flux measurements shown in Fig. 14 and Fig. 15 are 4 second averages.

D. The March 3 Observation, Fig. 14

A simultaneous enhancement of the intensity of VLF electromagnetic radiation, auroral optical emission, and precipitated electrons is evident in the March 3 observation, Fig. 14. The VLF spectrum analyzer indicates that the emission spectrum is essentially a flat noise spectrum starting below 2.7 kc/s and extending above 8.8 kc/s. The response of the 4.3 kc/s and 5.5 kc/s spectral density channels, during this event, is similar in character and amplitude to the response of the 2.7 kc/s, 5.5 kc/s, and 8.8 kc/s channels. The 4.3 kc/s and 5.5 kc/s channels have not, therefore, been shown in Fig. 14. A piecewise integration of the VLF magnetic spectral density using the spectrum analyzer measurement gives calculated rms wide-band magnetic signal strengths in good agreement with the (A.G.C.) wide-band signal strength measurements. We identify the VLF emission occurring in this event as an auroral hiss emission on the basis of the characteristic wide-band noise spectrum and the close association between the VLF hiss and the auroral optical emissions. The following points will be made concerning the association between the VLF emission, the auroral optical emission, and the

precipitated electrons as seen in the temporal scale of the satellite during the March 3 event. Reference will be made to the L shell parameter as a coordinate. It must be remembered, however, that it is not possible to separate temporal and spatial dependences in this observation. First, a general enhancement of VLF hiss and optical emission at 3914 Å, above the respective background noise levels, occurs very nearly coincident at an L value of 6. At this point the precipitated flux is in general increasing. Second, the enhancement of VLF hiss at L = 6 is very abrupt. The magnetic spectral density at 5.5 kc/s increases by two orders magnitude in 10 seconds or 80 km translational distance. Such an abrupt enhancement is not apparent in either the precipitated particle flux or the auroral optical emission. Third, after the onset of the VLF hiss, the magnetic spectral density measurements show rapid temporal fluctuations (less than 2 seconds) often exceeding one order of magnitude. The average magnetic spectral density, averaged for 10 seconds, is nearly constant to within one order of magnitude (10^{-8} to 10^{-9}(gamma)^2(c/s)$^{-1}$) over a range of L values from L = 6 to L = 14. The variations in the intensity of the optical emission and the precipitated particles, however, exceed two orders of

magnitude over the range of L values from L = 6 to L = 14. It appears, therefore, that the dynamic changes in the precipitated particle flux and the auroral optical emissions are not strongly coupled with the VLF hiss intensity as viewed by the satellite moving through space and time. Fourth, after the occurrence of the maximum auroral emission the intensity of the VLF hiss radiation observed at the satellite decreases to the receiver noise level without an abrupt change in intensity as observed at the L = 6 hiss onset. Fifth, the hiss intensity did not show a strong decrease at the time of maximum auroral activity. This observation serves to support the proposition mentioned earlier that decreases in VLF auroral hiss, observed on the ground, during the presence of intense and active aurorae are attributable to the attenuation of the VLF hiss radiation in the lower ionosphere.

From the event illustrated in Fig. 14, showing the simultaneous occurrence of VLF emission, auroral optical emission, and particle precipitation, it seems plausible that the auroral hiss is associated with the corpuscular streams which excite the auroral optical emissions. The period of time during which auroral

emissions were detected in the March 4 observation was 3 minutes. We shall now assume that the variations in the phenomena observed in the March 4 event were small for times on the order of 3 minutes. This assumption is considered plausible because the time scale associated with the development phase of an aurora is usually much larger than 3 minutes. The time scale of auroral variations during the break-up phase are, however, often much less than 3 minutes. The development phase of the aurora is usually much longer than the break-up phase. It would appear, therefore, that it is probable that the March 4 observation was not made during the break-up of the aurora and that the time scale associated with the event was long compared to 3 minutes.

Using the assumption that the phenomena observed in the March 4 event were time-stationary for times on the order of 3 minutes, the VLF measurements in Fig. 14 are interpreted as giving the spatial extent of the ionosphere illuminated by the VLF hiss radiation. We shall now compare the geomagnetic L shell boundaries of the precipitated particle stream with the L shell boundaries of the hiss radiation. This comparison will be made from measurements at the satellite altitude of approximately 300 km. For a given phenomenon we shall

define the position of the L shell boundary, at a constant altitude, to be those points where the intensity measurements associated with the phenomenon are one-tenth of the peak intensity occurring. These bounds may be considered as defining a region, at the satellite altitude, upon which the major fraction of the energy associated with a phenomenon is incident. The precipitated particle flux measurement obtained with detector 5 and the auroral optical emission may be taken as a measure of the intensity of the precipitated particle stream exciting the aurora. Each of these measurements has limitations in defining the intensity of the precipitated particle stream. Detector 5 is not sensitive to electrons $E \leq 40$ kev. and protons $E \leq 500$ kev.; hence, it is quite possible that a large portion of the precipitated particles are not energetic enough to be seen by this detector. [Private communication, B. J. O'Brien, Rice University]. Using the auroral optical emission as an index of the precipitated particle flux has the difficulty that the transformation from optical emission intensity to particle flux is not known.

The L shell boundaries of the precipitated particle stream in the March 3 event were roughly estimated using

the response of detector 5 and the intensity of the auroral optical emission. The estimated bounds (one order of magnitude below the peak intensity) of the precipitated particle flux is shown as $\delta\Lambda_p$ in Fig. 14. The estimated bounds of the VLF hiss radiation are shown as $\delta\Lambda_h$ in Fig. 14. An order of magnitude change in the magnetic spectral density has been taken to be a factor of $(10)^{1/2}$ in the wide-band VLF signal strength. Expresed in terms of invariant latitude Λ, $L\cos^2\Lambda = 1$, the spatial extent of the hiss illuminating the lower ionosphere, determined using the above bounds, was approximately $\delta\Lambda_h = 9.5$ degrees. The spatial extent of the particles being precipitated into the atmosphere, as determined from detector 5 and the auroral optical emission, using the previously defined boundary criterion, was approximately $\delta\Lambda_p = 3.3$ degrees. It appears, therefore, that the region of the ionosphere illuminated by the major fraction of the VLF hiss energy is approximately three times as large, in terms of invariant latitude, as the region of the atmosphere into which the major fraction of the particles are being precipitated. If it is assumed that the VLF hiss is generated within the L shell boundaries of the precipitated particle stream, it would appear that

the VLF hiss emission must occur at sufficiently high altitudes that the VLF radiation can illuminate a range of Λ values, at the satellite altitude, considerably larger than the range of Λ values over which particles are being precipitated into the atmosphere.

E. The February 28 Observation, Fig. 15

A simultaneous enhancement of the intensity of VLF electromagnetic radiation, auroral optical emission, and precipitated electrons is also evident in the February 28 observation, Fig. 15. The auroral optical emissions occurring in this observation are of a more complex nature than the auroral emission occurring in the March 3 event. As observed in the temporal coordinate associated with the motion of the satellite through time and space, a slowly varying optical emission can be distinguished having a maximum at approximately L = 7.5 and extending from L = 6 to L = 14. In addition, three sharply defined emission peaks can be seen, one peak occurring at L = 9.5 and the other two occurring at approximately L = 12. The VLF spectrum analyzer indicates that the VLF radiation detected at the satellite is a noise spectrum extending over a wide range of frequencies. The magnetic spectral density shows marked variations with time. These variations indicate that the frequency spectrum of the VLF hiss radiation at the satellite is changing with the motion of the satellite through space and time. The spectral density tends to increase at higher frequencies. We

identify the VLF emission as an auroral hiss emission on the basis of the characteristic wide-band noise spectrum and the association with the auroral optical emissions. From the wide-band signal strength measurement, it appears that the VLF hiss is closely associated with the sharp auroral emission peaks but it is not closely related to the slowly varying auroral emission extending from L = 6 to L = 14. The precipitated particle flux shows a general enhancement occurring with the slowly varying optical emission. Peaks in the particle precipitation can be roughly associated with the sharp auroral emission peaks.

We shall now assume that the variations illustrated in Fig. 15 display primarily the spatial extent of the phenomena considered. Using this assumption we identify the sharp auroral peaks as an intensity cross-section through an auroral arc or band. Auroral arcs have been described by Chamberlain as "a luminous arch usually stretching from magnetic east to west with its highest point near the magnetic meridian". [Chamberlain, 1961.] The wide-band VLF signal strength shows good correlation between the spatial position of the auroral arcs and the intensity of VLF radiation observed at the satellite.

The intensities of the peak optical emissions occurring at L = 9.5 and L = 12 differ by a factor of four. The amplitude of the wide-band VLF signal strength measurement is, however, very nearly the same for these two L values. The VLF spectrum analyzer indicates that the frequency spectrum of the hiss emission is considerably different at L = 9.5 and L = 12. The VLF hiss associated with the first arc at L = 9.5 extends from 4.3 kc/s to greater than 8.8 kc/s. (The hiss is just detectable in the 4.3 kc/s channel, not shown in Fig. 15.) The magnetic spectral density is increasing with increasing frequency. The VLF emission associated with the arcs occurring at approximately L = 12 has a relatively flat noise spectrum extending from less than 2.7 kc/s to greater than 8.8 kc/s. Morozumi has found from ground-based observations that VLF hiss was not characteristic of all aurorae but has a special association with auroral arcs and bands. The observations shown in Fig. 15 may be interpreted as providing an illustration of the association between VLF hiss and auroral arcs.

CONCLUSION

Two major assumptions were used in the interpretation of the data from the Injun III VLF experiment.

A. It must be assumed that the motion of the satellite through the magnetospheric medium does not generate detectable VLF emissions or enhance naturally occurring VLF emissions.

B. In the interpretation of the absolute amplitude measurements, it must be assumed that, for a VLF electromagnetic field in an ionized medium, the satellite shell represents a negligible perturbation on the VLF magnetic field measurement obtained from the loop antenna.

A weak argument, based on the fact that the spectral character of VLF phenomena observed with Injun III is not unlike those commonly observed with ground-based VLF receivers, has been used to support the first assumption. It has not been possible at the present time to establish the validity of these assumptions on experimental grounds. A theoretical treatment of these assumptions may prove to be profitable but has not been attempted in this paper.

VLF measurements in the ionosphere with Injun III have been characterized by remarkably large VLF magnetic intensities relative to ground-based measurements. Only three whistlers and no VLF emissions were detected on the ground with the satellite VLF receiver and antenna for a total observation time of 15 hours, extending over a two month period. The same VLF receiver and antenna in orbit has detected many long hop whistlers and has detected magnetospheric VLF emissions for 24 percent of the total observation time during January, 1963. On one occasion, a wide-band VLF hiss emission was observed in the ionosphere for which the magnetic spectral density of the hiss radiation was 3.6×10^{-7} $(\text{gamma})^2(\text{cps})^{-1}$. This spectral density was a factor of 10^6 greater than the maximum observed on the ground, in previous studies of a similar phenomena, by Ellis.

A notable exception to the generally large VLF intensities observed at the satellite, is the background noise level of spheric impulses (short fractional-hop whistlers). The spheric background noise level is much lower in the upper ionosphere than on the ground. These observations may be attributed, in part, to the ionospheric attenuation of electromagnetic waves at VLF frequencies. It seems probable, in the case of VLF magnetospheric

emissions, that additional factors may be operating which increase the intensity of the magnetic component of the VLF radiation, relative to ground-based observations. It has been suggested, for instance, that ducting of VLF radiation may occur in the magnetosphere. A very intense VLF power flux may be observed when the satellite is in a propagation duct or in close proximity to the source of the VLF emission.

Hiss having frequencies less than 1 kc/s and chorus are the most common VLF electromagnetic emissions observed at the satellite. ELF hiss having frequency components as low as 200 c/s is commonly observed at the satellite and is often characterized by a sharply defined upper frequency limit. The frequency response characteristics of the VLF receiver have made absolute measurements in this frequency range difficult.

Direct measurements of the amplitude of the VLF radiation from chorus emissions have been made in the ionosphere with Injun III. These measurements have been analyzed for satellite local time coordinates between 0800 and 1300. The measurements analyzed extended over a three day period. The amplitude of the chorus radiation at the satellite was found to have a systematic

variation with the geomagnetic L parameter. This variation was highly reproducible from pass to pass. The amplitude of the VLF chorus radiation illuminating the ionosphere shows a well defined peak at L = 5 for the three day period studied. The amplitude of the magnetic component of the VLF chorus radiation at L = 5 was typically 8×10^{-3} gamma in the frequency band 0.5 to 7.0 kc/s.

When the frequency-time spectra of the chorus radiation was compared at the same L value for different passes, the character of the spectra was found to vary markedly in times less than one orbit period. Chorus emissions have been observed for which the discrete emissions occur over a narrow band of frequencies. In some instances, the center frequency of banded chorus emissions is found to be remarkably independent of L. This observation suggests that the VLF radiation from the same chorus source region was being viewed by the satellite VLF antenna over a wide range of L values.

Simultaneous occurrences of VLF hiss emission, auroral optical emission, and particle precipitation into the atmosphere have been observed on several occasions with Injun III. Two specific observations

have been presented in this paper. These observations occurred on February 28 and March 3, 1963. It was not possible in either of these observations to resolve the auroral optical intensity variations viewed by the satellite into spatial and temporal variations associated with the aurora. In the interpretation of the two observations presented it was assumed that the phenomena being observed were time-stationary for times on the order of the total observation from the satellite. Using this assumption and the fact that the photometer axis was closely aligned with the geomagnetic $\vec{B}$ field the intensity variations in the auroral photometer, the VLF experiment, and detector 5 were interpreted as giving the spatial variations of the auroral optical intensity, the intensity of the VLF hiss radiation, and the particle flux precipitated into the atmosphere. The magnetic spectral density of the VLF hiss occurring at the satellite during these two events was on the order of $10^{-8}(\text{gamma})^2 (\text{c/s})^{-1}$.

For the auroral event observed with Injun III on March 3, 1963 it was found that the region of the ionosphere illuminated by the major fraction of the VLF

hiss energy is approximately three times as large, in terms of invariant latitude, as the region of the atmosphere into which the major fraction of the particles were being precipitated. The intensity of the auroral optical emission and detector 5 were used to roughly define the boundaries of the precipitated particle stream.

For the auroral event observed with Injun III on February 28, 1963 it was found that the VLF hiss intensity observed at the satellite was closely associated with sharp auroral optical intensity peaks. The VLF hiss was not closely associated with an auroral optical emission extending from L = 6 to L = 14 for which intensity varied slowly with latitude. If the sharp auroral intensity peaks are interpreted as auroral arcs or bands this observation may be used to support an earlier observation by Morozumi. He found ground-based observations that the VLF hiss was not characteristic of all aurorae but has a special association with arcs and bands.

APPENDIX

A. Electromagnetic Waves in a Magneto-Ionic Medium

We shall briefly discuss the nature of electromagnetic wave propagation in a magneto-ionic medium. We shall also consider the detection of such a wave with a loop antenna, for geometries similar to those used in Injun III. A magneto-ionic medium consists of a statistically homogeneous mixture of free electrons, and neutralizing heavy positive ions, in the presence of a uniform magnetic field. [Ratcliffe, 1958]. The medium in the ionosphere and magnetosphere is not a homogeneous medium nor is the geomagnetic field uniform. The propagation of electromagnetic waves in the ionosphere and magnetosphere medium is, however, often studied using the magneto-ionic model.

The magneto-ionic model has been extensively used in the study of electron densities in the lower ionosphere and has to a good approximation been applicable to the propagation of whistlers in the magnetosphere.

The following quantities are defined (MKS units).

(1) Poynting Vector, $\vec{S}$: $\vec{S} = \vec{E} \times \vec{H}$.

(2) Ray direction $\vec{s}$: The direction of mean (time average) energy flow.

$$\vec{s} = \langle \vec{E} \times \vec{H} \rangle$$

(3) Phase normal $\vec{K}$: A vector in the direction normal to the planes of constant phase of $\psi(r,t)$, where

$$\psi(r,t) = A(\vec{r}) \exp[j(\omega t - \vec{K}\cdot\vec{r})]$$

(4) Phase velocity v_p: The velocity at which a condition of constant phase moves in the $\vec{K}$ direction.

(5) Index of refraction n: $n = c/v_p$, note that n may depend upon the direction of K.

(6) Group velocity v_g: The velocity which a wave packet propagates in the medium.

$$v_g = c\left(n + \omega \frac{dn}{d\omega}\right)^{-1}$$

(7) Gyro-frequency ω_H: A characteristic frequency associated with the ith plasma constituent of mass m_i.

$$\omega_H = \frac{eB_o}{m_i}$$

(8) Plasma-frequency ω_p: A characteristic frequency of a plasma having electron density n_e.

$$\omega_p^2 = \frac{N_e e^2}{\epsilon_o m_e}$$

B. The Appleton-Hartree Formula

The Appleton-Hartree dispersion relation may be used to calculate the index of refraction in a plasma under the influence of a uniform magnetic field. [See Brandstatter, 1963.] In general the index of refraction is double valued and is a function of the angle θ between $\vec{K}$ and the uniform magnetic field $\vec{B}_o$. The double-valued feature of the index of refraction expression arises because the phase velocity in the medium is dependent upon the polarization of the wave. The two modes of propagation are called the ordinary and extraordinary modes. The Appleton-Hartree formula for the index of refraction for the extraordinary mode when $\vec{K}$ and $\vec{B}_o$ are parallel is given by:

$$(9) \qquad n^2 = 1 + \frac{\omega_p^2}{\omega(\omega_H - \omega)}$$

An expression for the group velocity for this case, when $\omega_p^2 \gg \omega_H \omega$, is given by

$$(10) \qquad v_g = 2c \frac{\omega^{1/2} (\omega_H - \omega)^{3/2}}{\omega_H \omega_p}$$

These relationships are in general applicable to whistlers and other VLF radiation propagating approximately parallel to the geomagnetic $\vec{B}$ field. The guiding effect, of the geomagnetic $\vec{B}$ field on the ray direction of whistlers in the magnetosphere, arises from the variation in the index of refraction with θ. If $n(\theta)$ is plotted in polar coordinates it can be shown that the ray direction for given θ_1 is normal to the $n(\theta)$ curve at $\theta = \theta_1$. When the effects of positive ions are ignored the ray-direction must lie within a cone whose axis is parallel to $\vec{B}_o$ and whose half-angle is less than approximately 20°. [Storey, 1953].

C. The Loop Antenna in a Plasma

The magnetic component of an electromagnetic field in a plasma may be detected with a loop antenna. In the case of the Injun III loop antenna the radius of the antenna b was much less than the wavelength of the VLF radiation being detected. The plane of the Injun III loop antenna is known to be approximately parallel with geomagnetic $\vec{B}$ vector (after the oscillations associated with injection into orbit had damped.)

Brandstatter makes the following comments concerning the fields in a uniform plasma [Brandstatter, 1963]:

(a) "The plasma in a uniform magnetic field is always doubly refracting."

(b) "The fields associated with each mode of propagation can be resolved into a linearly polarized component parallel to the uniform magnetic field and two oppositely rotating circularly polarized components whose plane of rotation is perpendicular to the direction of the uniform magnetic field."

(c) "The two fields associated with the different modes of propagation are completely independent."

(d) For a given initial angle Θ between the phase normal $\vec{K}$ and the uniform magnetic field, the $\vec{K}$ vector is, thereafter, confined to a cone whose axis is parallel to the uniform magnetic field and having a half-angle Θ. The $\vec{K}$ vector traverses the rim of the above cone as the phase of the circularly polarized components change.

An illustration showing the relative geometries of the fields associated with an electromagnetic wave in a plasma are shown in Fig. 16. The Poynting vector, $\vec{S} = \vec{E} \times \vec{H}$, moves round the surface of the cone shown. As the phase of the circularly polarized components

change, the $\vec{K}$ vector moves round the $\vec{B}_o$ field with the angle θ remaining constant.

If $\vec{n}$ is a unit vector perpendicular to the plane of a loop antenna having N turns and area A, the emf induced in the antenna by the electromagnetic field is given by the expression below when the wavelength is much larger than the antenna dimensions.

(11) $v = NA \frac{d}{dt} [\vec{B} \cdot \vec{n}]$; $\vec{B} = \mu_o \vec{H}$

or if $\vec{B} \cdot \vec{n} = B_p \exp[j\omega t]$

(12) $v = j\omega NA B_p \exp[j\omega t]$

The relative geometrics of the electromagnetic fields and the loop antenna, as used on Injun III, are shown in Fig. 16. From item (b) above, we note that the emf induced in the Injun III antenna can be interpreted as arising from the circularly polarized H component whose plane of rotation is perpendicular to the direction of the uniform magnetic field. This interpretation will be used in the analysis of the Injun III VLF measurements. It is not known to what extent the presence of the satellite shell near the loop antenna perturbs the electromagnetic field coupling the loop.

D. Calibration of the VLF Experiment

A block diagram of the VLF experiment is shown in Fig. 4. No attempt will be made to discuss the detailed electrical operation of the instrument. The VLF experiment will be viewed as a black box having a single input, an analog signal output, and seven quantized digital outputs. The input will be a magnetic field spectrum applied perpendicular to the plane of the antenna (i.e., $\vec{B}\cdot\vec{n}$ in the previous discussion). The calibration of the instrument will be considered as a description of the dependence of the various outputs upon the parameters describing the input signal.

The functional elements in the VLF experiment are shown in Fig. 4. A brief description of the operation of each element will be presented before the detailed calibration of the experiment is discussed. The electrical stimulus for the VLF electronics is the very small emf induced in the antenna by the VLF electromagnetic field. The amplitude of the emf for a constant rms amplitude of $\vec{B}\cdot\vec{n}$ is proportional to the wave frequency ω. We wish to interpret the VLF measurements in terms of the spectral character of $\vec{B}\cdot\vec{n}$. It would be convenient, therefore, to correct for the frequency response of the antenna. The preamplifier includes a network having a

frequency response proportional to $(\omega)^{-1}$. The output amplitude of the preamplifier signal for a constant rms amplitude of $\vec{B}\cdot\vec{n}$ is, therefore, independent of the wave frequency ω.

The preamplifier signal, limited to a frequency band of approximately 0.5 - 7.0 kc/s, is normalized to a constant amplitude by an automatic gain control (A.G.C.) circuit. This normalized signal is used to phase-modulate (PM) the 1.5 watt telemetry transmission at 136.860 Mc/s. Normalization of the modulation signal amplitude is necessary to efficiently modulate the telemetry transmission. When the satellite transmission at 136.860 Mc/s is demodulated with a receiver, the receiver analog output signal has a frequency spectrum faithfully reproducing the spectral character of $\vec{B}\cdot\vec{n}$ in the 0.5 - 7.0 kc/s frequency range. The relative frequency response of the wide-band VLF system, including the antenna, preamplifier, A.G.C. circuit, PM transmitter and receiver, is shown in Fig. 5. This measurement was made by holding the gain of the A.G.C. circuit constant. Since the frequency response of the transmitter and receiver system are very nearly independent of frequency (in the range considered), Fig. 5 gives essentially the frequency response

of the A.G.C. circuit for constant gain. Absolute amplitude information is destroyed by the A.G.C. circuit in the VLF analog transmission. The A.G.C. feedback voltage, however, provides a measure of the wide-band absolute signal strength from the preamplifier. The frequency response of the A.G.C. circuit (Fig. 5) provides the proper weighting function for this measurement at different frequencies. The A.G.C. circuit time constant is approximately 0.2 seconds. The wide-band signal strength measurement (A.G.C. feedback voltage) is sampled instantaneously at 4 second intervals by an analog to digital converter. The output from the wide-band signal strength measurement is, therefore, representative of the magnetic spectral density integrated over the receiver bandwidth using the frequency response curve shown in Fig. 5.

The VLF spectrum analyzer provides measurements of the magnetic spectral density of the VLF electromagnetic wave coupling the loop antenna at six frequencies. In the spectrum analyzer the frequency spectra from the preamplifier is translated upwards in frequency by 100 kc/s. The spectrum analyzer channels are defined with magnetostriction filters. The 3db bandwidth of each filter

is approximately 50 c/s. The amplitude of the signal in each channel is measured by an envelope detector. The dynamic range over which the detector is linear is approximately 40 db. To provide an extended dynamic range an attenuator was included between the preamplifier and the spectrum analyzer. The dynamic range may be shifted in two 20 db steps by remote commands from the ground. The amplitude measurementfrom the envelope detector is processed by an analog to digital converter which generates a number proportional to the logarithm of the minimum amplitude occurring in the time interval since the previous sample was transmitted. The analog to digital converter has sixteen quantizing steps. The 40 db dynamic range of the spectrum analyzer is, therefore, quantized into sixteen steps, approximately 2.5 db per step. The measurement of the minimum amplitude over a period of time was used in order that the spectrum analyzer measurement would give the amplitude of the slowly varying noise spectrum ($\tau \gtrsim 2$ seconds) and would ignore transient noise impulses ($\tau \lesssim 0.1$ sec) like lightning. The sampling rate most commonly used in orbit is one sample every two seconds.

To calibrate the VLF experiment we must choose parameters descriptive of the VLF magnetic component $(\vec{B}.\vec{n})$ detected with the antenna. Because the spectral nature of many VLF emissions (especially hiss) closely resembles a banded noise spectrum, it was decided that random noise would be used to calibrate the absolute amplitude measurements. Random noise signals are usually described by a spectra density G(f). $G(f)\,\Delta f$ is the average power or mean-square signal in the frequency interval Δf. We shall use B(f) to denote a magnetic spectral density. We shall define the rms signal strength B_r by the relation

$$(13) \qquad B_r^2 = \int B(f)\,df$$

The spectral power density of an electromagnetic wave in a nonconducting medium having index of refraction n is given in terms of B(f) and B_r as

$$\vec{S} = \vec{E} \times \vec{H}$$

$$(14) \qquad S = \frac{1}{n}\sqrt{\frac{\mu_o}{\epsilon_o}}\left(\frac{B_r}{\mu_o}\right)^2 \qquad \text{watts (m)}^{-2}$$

$$(15) \qquad S(f) = \frac{1}{n}\sqrt{\frac{\mu_o}{\epsilon_o}}\,\frac{B(f)}{\mu_o^2} \qquad \text{watts (m)}^{-2}\text{(c/s)}^{-1}$$

The units used for B(f) will be $(\text{gamma})^2(\text{c/s})^{-1}$ ($1 \text{ gamma} = 10^{-9} \text{ weber(m)}^{-2}$). The units used for B_r will be rms gamma.

It was decided that the spectrum analyzer channels and the wide-band signal strength measurement would, in principle, be calibrated by applying a constant spectral density, magnetic noise signal, $B_o(f)$ normal to the plane of the loop antenna. The spectrum analyzer calibration is, therefore, the dependence of the digital readout, from each spectrum analyzer channel, upon the applied magnetic spectral density $B_o(f)$. For the wide-band signal strength a slightly different interpretation of the applied stimulus is used. For a given constant magnetic spectral density $B_o(f)$ applied to the antenna, we shall assign to the wide-band signal strength digital readout a quantity given by $B_W = [B_o(f)\,\Delta f]^{1/2}$, $\Delta f = 7$ kc/s. B_W will be called the wide-band magnetic field strength. The noise band width Δf of a circuit is defined as the band-width of an ideal rectangular passband, having the same maximum gain and passing the same average power, from a white-noise source, as the circuit under consideration, [J. C. Hancock, p. 150, 1961]. The noise band-width Δf for the A.G.C. circuit

was determined, by graphical integration of the frequency response of the A.G.C. circuit (Fig. 5), to be approximately 7 kc/s. The wide-band magnetic field strength B_W will be interpreted as the square root of the integral given in equation 13, integrated from 0-7 kc/s. B(f) is the spectral density of the $\vec{B}\cdot\vec{N}$ component at the loop antenna. The error implicit in this interpretation is given by the frequency response of the A.G.C. circuit shown in Fig. 5. Above 1 kc/s the maximum error in this interpretation is about 4 db. Below 1 kc/s the error in this interpretation becomes progressively larger.

A direct calibration of the VLF experiment at maximum sensitivity by applying a magnetic field to the antenna is impossible because of the continually present spheric and power system noise. The Injun III VLF experiment was calibrated by using an electrical analog of the VLF antenna. The network was designed such that the electrical input voltage signal was directly analogous with the $\vec{B}\cdot\vec{N}$ component. The electrical analog of the antenna is shown in Fig. 17. The 1.6 mh inductance and the 0.8Ω resistance correspond to the inductance and resistance of the loop antenna (distributed capacitance effects were negligible.) The response of the RC network to a signal of angular frequency ω is given by $v = j\omega RCV_1$,

when $RC\omega \ll 1$. If we compare this expression with equation 12 we may establish the following analogy.

$$(16) \quad B_r = \frac{RC}{NA} V_1 \; ; \quad RC\omega \ll 1$$

or in terms of spectral densities

$$(17) \quad B(f) = \left(\frac{RC}{NA}\right)^2 G_1(f) \; ; \quad RC\omega \ll 1$$

The relationship in equation 17 follows from equation 16 as a result from linear network theory. [Hancock, p. 124, 1961]. The voltage spectral density $G_1(f)$ shown in the diagram of the VLF calibration (Fig. 17) may, therefore, be interpreted as a magnetic spectral density applied to the antenna, had the antenna been connected to the VLF instrument. The values for C and R were measured on an audio frequency bridge and were found to be C = 0.101 μf $\pm$ 1% and R = 0.203 ohm $\pm$ 1%, clearly $RC\omega \ll 1$. The quantities N and A are also known so B(f) can be calculated if $G_1(f)$ is measured.

The spectral density of the white noise source, used in the VLF calibration, was measured at various frequencies with a Donner wave analyzer and found to be constant to within $\pm$ 1.0 db. over the frequency range considered. The spectral density $G_o(f)$ was measured,

during the calibrations, by measuring the true rms voltage at the output of a low-pass-filter (LPF) having a sharp cutoff at 7 kc/s. A variable attenuator was used to control the amplitude of $G_1(f)$. The output of the VLF experiment consisted of a sequence of numbers from the six spectrum analyzer channels and from the wide-band signal strength measurement. Since the signal being measured is random noise, the digital outputs from the VLF experiment have random fluctuations. Using a random noise input signal, the standard deviation of the spectrum analyzer digital readout was found to be approximately $\sigma = 0.37$ units. The digital measurements from the spectrum analyzer were averaged for approximately 20 successive samples during the calibration of the instrument. The calibration of the spectrum analyzer channels at 25°C are shown in Figures 18 through 23. The receiver noise level can be estimated, at each of the six frequencies, from the break in the curves at low signal levels. The receiver noise level is approximately $5.0 \times 10^{-11}(\text{gamma})^2(\text{c/s})^{-1}$. Using this noise level and equation 15 with n = 1, the receiver noise level, in terms of the VLF power spectral density detectable on the ground, is approximately 1.5×10^{-14} watts$(\text{m})^{-2}(\text{c/s})^{-1}$. In general it can be seen that the receiver noise level

increases at lower frequencies, especially the 700 c/s channel. The variations in the analyzer gain and receiver noise level with temperature are shown in Table I. The numbers shown in the table are the decimal readouts for the various frequency channels averaged for approximately 20 successive samples. The results of the calibration of the wide-band magnetic signal strength measurement have been shown in Fig. 4. The variations in these measurements with temperatures from 10°C to 25°C were on the order of the quantizing errors associated with the measurement.

E. The Performance of the VLF Experiment in Orbit

It is desirable to check the calibration of the VLF experiment periodically in flight. No system was included in the Injun III VLF experiment for postlaunch calibrations. A good check can be made on the absolute gain of the instrument by comparing the receiver noise levels in flight with those noted in the preflight calibrations. Receiver noise levels, in terms of the digital readouts from the spectrum analyzer channels, are shown for several postlaunch dates in Table 1. These measurements are the average of 20 successive readouts for conditions when no VLF radiation was thought to be detectable. The 700 c/s channel has shown a consistently higher noise level in flight than in the prelaunch calibrations. It is not known whether these measurements are indicative of VLF radiation being detected at this frequency or whether the gain of this channel has in fact shifted. The 700 c/s channel has shown good correlation with the wide-band signal strength measurements for cases where the VLF emissions were less than 1 kc/s. A large percentage of the time the 700 c/s channel is saturated, possibly indicating strong VLF signals at this frequency. The validity of the calibration

of the 700 c/s channel cannot be established at this time. The remaining spectrum analyzer channels show postlaunch noise levels in good agreement from month to month, and possibly slightly higher (less than 2.5 db) than the prelaunch calibrations. The receiver noise level measurement in orbit with the wide-band VLF signal strength measurement has in every case read 3, in agreement with the prelaunch calibrations. (See Fig. 24). Checks of the A.G.C. calibration relative to the spectrum analyzer calibration, by piecewise integration of the magnetic spectral density of wide-band hiss events, have shown, in general, agreement to within $\pm$ 2.5 db. In view of the uncertainty associated with the perturbation caused by the satellite shell on the absolute measurement of the VLF field, the instrumental calibration errors have not been stated in the results presented.

REFERENCES

1. Allcock, G. Mck., "A Study of the Audio-Frequency Phenomena Knows as 'Dawn Chorus'," Aust. J. Phys., Vol. 10, p. 286, 1957.

2. Allcock, G. Mck, and Martin, L. H., "Simultaneous Occurrence of 'Dawn Chorus' at Places 600 Km. Apart," Nature, Vol. 178, p. 937, Oct. 27, 1956.

3. Barrington, R. E. and Belrose, J. S., "Preliminary Results from the VLF Receiver Aboard Canada's Alouette Satellite," Goddard Space Flight Center Publication X-615-63-36, 1963.

4. Brandstatter, Julius J., An Introduction to Waves, Rays, and Radiation in Plasma Media, McGraw-Hill Book Co., Inc. 1963.

5. Cain, J. C., Shapiro, I. R., Stolarik, J. D., Heppner, J. P., "A note on whistlers observed above the ionosphere," J. Geophys. Research, Vol. 66, No. 9, Sept., 1961.

6. Chamberlain, J. W., Physics of the Aurora and Airglow, Academic Press, 1961.

7. Dowden, R. L., "Doppler Shifted Cyclotron Generation of Exospheric Very-Low Frequency Noise ("Hiss")," Planet. Space Sci., Vol. 11, No. 4, p. 361, April, 1963.

8. Ellis, G. R. A., "Low Frequency Electromagnetic Radiation Associated with Magnetic Disturbances," Planet. Space Sci., Vol. 1, p. 253, 1959.

9. Ellis, G. R. A., "Low-frequency radio emission from aurorae," Journal of Atmospheric and Terrestrial Physics, Vol. 10, p. 302, 1957.

10. Frank, L. A., Craven, J. D., Note on the Characteristics of the G.M. Detectors on Injun III, SUI Memo, March 11, 1963.

11. Gallet, R. M. and Helliwell, R. A., "Origin of 'Very-Low-Frequency Emissions'," Journal of Research of the National Bureau of Standards-D. Radio Propagation, Vol. 63D, No. 1, July-August, 1959a.

12. Gallet, R. M., "The Very-Low-Frequency-Emissions Generated in the Earth's Exosphere," Proceedings of the IRE, Vol. 47, No. 2, p. 211, February, 1959b.

13. Hancock, J. C., The Principles of Communication Theory, McGraw-Hill Book Company, Inc., 1961.

14. Helliwell, R. A. and Morgan, M. G., "Atmospheric Whistlers", Proceedings of the IRE, Vol. 47, No. 2, p. 200, February, 1959.

15. Helliwell, R. A., "Artificially Stimulated VLF Electromagnetic Radiation from the Earth's Atmosphere," Fall 1962, URSI Meeting at Ottawa, Canada, 1962a.

16. Helliwell, Stanford Electronics Lab Publication, 62-024, 1962b.

17. Hines, C. O., "Heavy-Ion Effects in Audio-Frequency Radio Propagation," Journal of Atmospheric and Terrestrial Physics, Vol. 11, No. 1, p. 36, 1957.

18. Jones, D. L., Gallet, R. M., Watts, J. M., Frazer, D. N., "An Atlas of Whistlers and VLF Emissions, A survey of VLF Spectra From Boulder, Colorado," National Bureau of Standards Technical Note No. 166, January, 1963.

19. Leiphart, J. P., "Penetration of the Ionosphere by Very-Low-Frequency Radio Signals--Interim Results of the LOFTI 1 Experiment," Proceedings of the IRE, Vol. 50, No. 1, p. 6, 1962.

20. Martin, L. H., and Helliwell, R. A., "Association Between Aurorae and Very-Low-Frequency Hiss Observed at Byrd Station, Antarctica," Nature, Vol. 187, p. 751, Aug. 1960.

21. Martin, L. H., "Whistlers in the Antarctic," Nature, Vol. 181, p. 1796, April, 1958.

22. Martin, T. L., Electronic Circuits, Prentice-Hall Inc., p. 231, 1951.

23. McIlwain, C. E., "Coordinates for Mapping the Distribution of Magnetically Trapped Particles," J. Geophys. Research, 66, No. 11, p. 3681, November, 1961.

24. Morgan, M. G., "Correlation of whistlers and lightning flashes by direct aural and visual observations," Nature, Vol. 182, p. 332, August 2, 1958.

25. Morozumi, H. M., "A Study of the Aurora Australis in Connection with and Association Between VLFE Hiss and Auroral Arcs and Bands Observed at the South Geographic Pole," Thesis, State University of Iowa, 62-14, 1962.

26. O'Brien, B. J., "A large variation of the geomagnetically trapped radiation," J. Geophys. Research, 68, No. 4, February, 1963.

27. O'Brien, B. J., Laughlin, C. D., and Gurnett, D. A., "The Injun III Satellite," State University of Iowa, 62-24, 1962a.

28. O'Brien, B. J., "Lifetimes of Outer-Zone Electrons and Their Precipitation into the Atmosphere," J. Geophys. Research, 67, No. 10, Sept. 1962b.

29. Pope, J. H., "Effect of Latitude on the Diurnal Maximum of 'Dawn Chorus'," Nature, Vol. 185, p. 87, January, 1960.

30. Ratcliffe, J. A., The Magneto-Ionic Theory and its Applications to the Ionosphere, Cambridge University Press, 1959.

31. Smith, R. L., Helliwell, R. A., and Yubroff, I. W., "A theory of trapping whistlers in field-aligned columns of enhanced ionization," J. Geophys. Research, 65, p. 815, 1960.

32. Smith, R. L., "Propagation characteristics of whistlers trapped in field-aligned columns of enhanced ionization," J. Geophys. Research, 66, No. 11, p. 3699, November, 1961.

33. Storey, L. R. O., "An Investigation of Whistling Atmospherics," Phil. Trans. Roy. Soc.,(A), Vol. 246, p. 113, July 9, 1953.

34. Ungstrup, E. and Jackeroh, I. M., "Observation of Chorus below 1500 Cycles per Second at Godhaven, Greenland, from July 1957 to December 1961, J. Geophys. Research, 68, No. 8, p. 2141, April, 1963.

	Prelaunch						Postlaunch					
Center Frequency	Absolute Gain vs Temperature Signal Input $1.2 \times 10^{-8}(\text{gamma})^2(\text{cps})^{-1}$			Receiver Noise Level vs Temperature			Date					
C/S	-5°C	10°C	25°C	-5°C	10°C	25°C	12/26/62	1/8/63	2/8/63	3/11/63	4/5/63	5/1/63
700	5.5	4.25	4.5	10.5	8.5	9.50	4.1	3.9	4.35	3.85	4.35	4.15
2,700	4.75	4.50	4.75	13.25	13.50	13.75	12.35	12.55	12.50	12.00	12.50	12.15
4,300	3.25	3.25	3.50	12.75	13.25	14.00	13.05	13.05	12.65	12.95	12.75	12.35
5,500	4.25	4.00	4.25	13.00	13.75	14.00	13.50	13.55	13.35	12.85	13.40	13.00
7,000	4.00	4.00	4.50	13.50	14.00	14.50	14.15	14.05	14.00	13.45	13.80	13.25
8,800	4.00	4.00	4.25	13.50	14.00	14.50	14.10	14.15	13.80	13.85	14.10	13.90

VLF Spectrum Analyzer Gain and Noise Level Variations

Table I

FIGURE CAPTIONS

Figure 1. Satellite Injun III.

Figure 2. Frequency-time spectrogram of a whistler.

Figure 3. High time resolution spectrograms of chorus at L = 4.

Figure 4. Block diagram - Injun III VLF Experiment.

Figure 5. Frequency response of the wide-band VLF system.

Figure 6. Low time resolution spectrogram of chorus.

Figure 7. Low time resolution spectrogram of chorus.

Figure 8. Viewing region of the VLF antenna.

Figure 9. Chorus observations in L and local time coordinates.

Figure 10. The amplitude of VLF chorus radiation versus satellite altitude.

Figure 11. The amplitude of VLF chorus radiation versus satellite altitude.

Figure 12. The amplitude of VLF chorus radiation versus local time at the satellite.

Figure 13. Narrow band chorus emissions at different L values.

Figure 14. The March 3, 1963 observation.

Figure 15. The February 28, 1963 observation.

Figure 16. The Injun III Loop Antenna and Electromagnetic Field Geometry.

FIGURE CAPTIONS (Continued)

Figure 17. Diagram - VLF experiment calibration.

Figure 18. Wide-band signal strength calibration.

Figure 19. Spectrum Analyzer Calibration - 700 c/s.

Figure 20. Spectrum Analyzer Calibration - 2.7 kc/s.

Figure 21. Spectrum Analyzer Calibration - 4.3 kc/s.

Figure 22. Spectrum Analyzer Calibration - 5.5 kc/s.

Figure 23. Spectrum Analyzer Calibration - 7.0 kc/s.

Figure 24. Spectrum Analyzer Calibration - 8.8 kc/s.

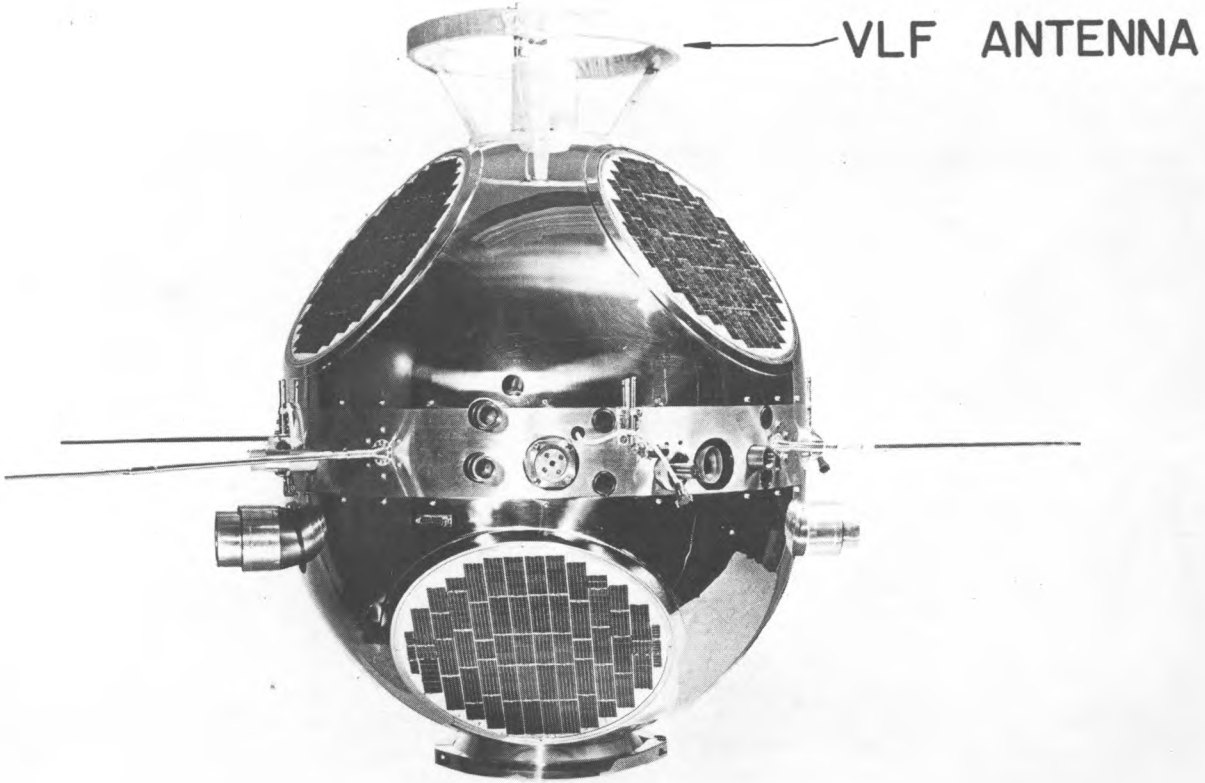

INJUN III

Figure 1

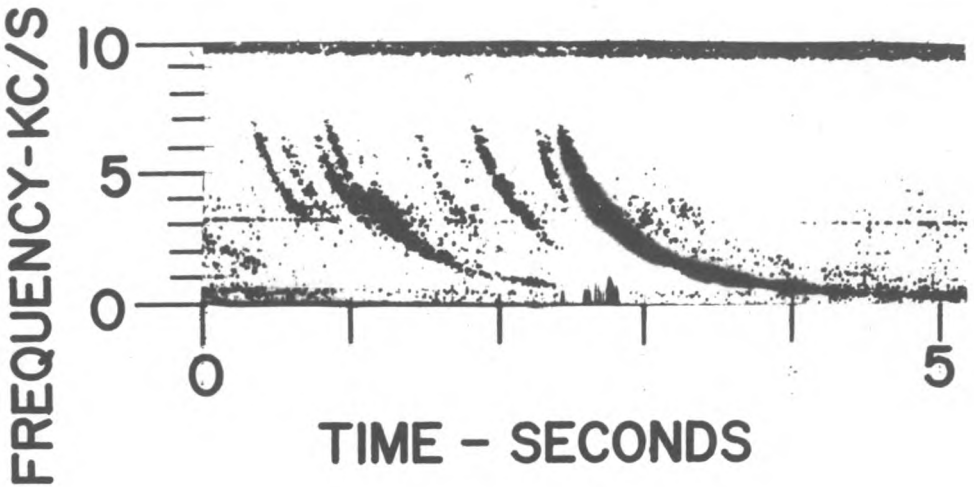

A SPECTROGRAM OF WHISTLERS OBSERVED WITH INJUN III

Figure 2

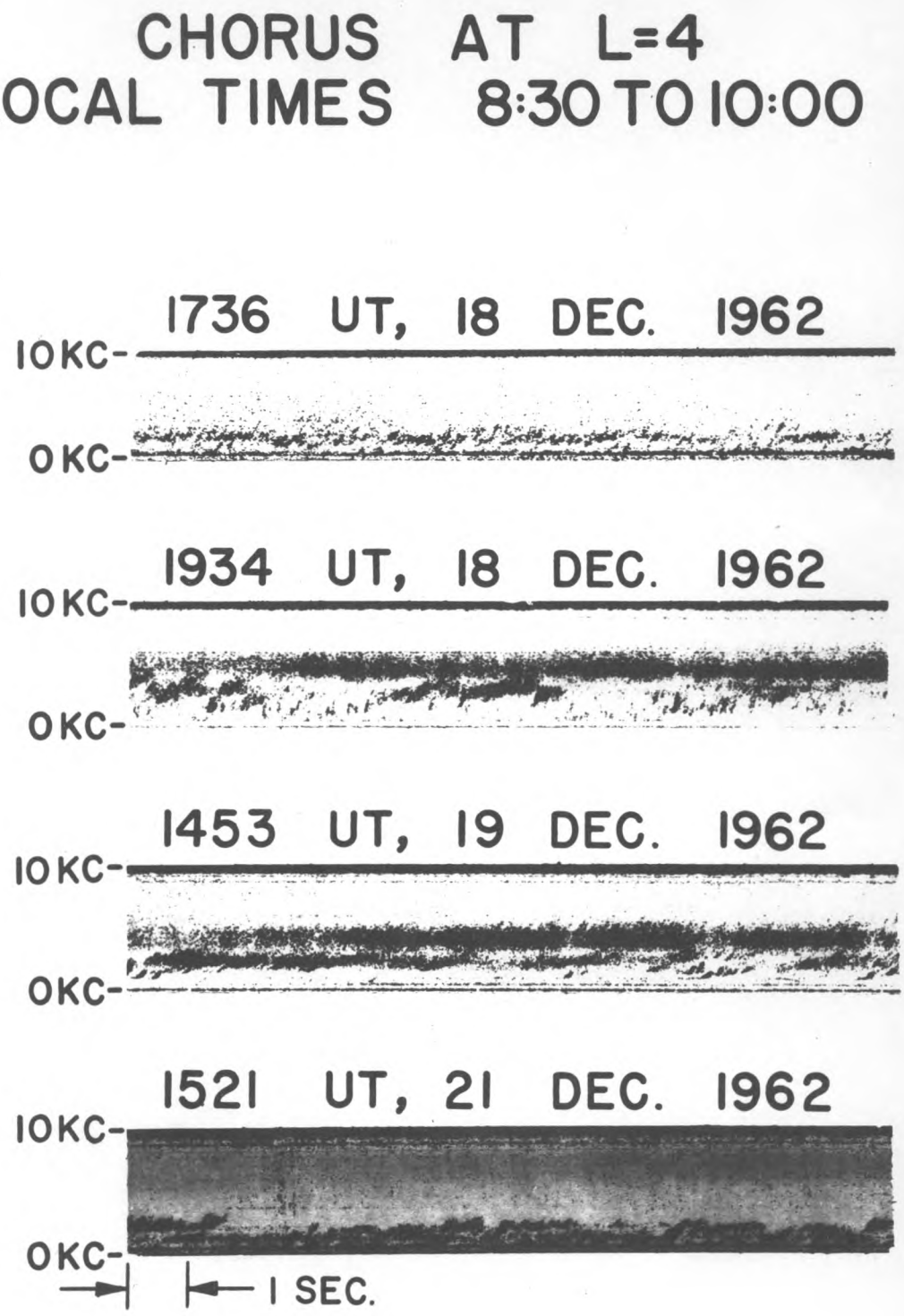
CHORUS AT L=4
LOCAL TIMES 8:30 TO 10:00
1736 UT, 18 DEC. 1962
10KC-
0KC-
1934 UT, 18 DEC. 1962
10KC-
0KC-
1453 UT, 19 DEC. 1962
10KC-
0KC-
1521 UT, 21 DEC. 1962
10KC-
0KC-
1 SEC.

Figure 3

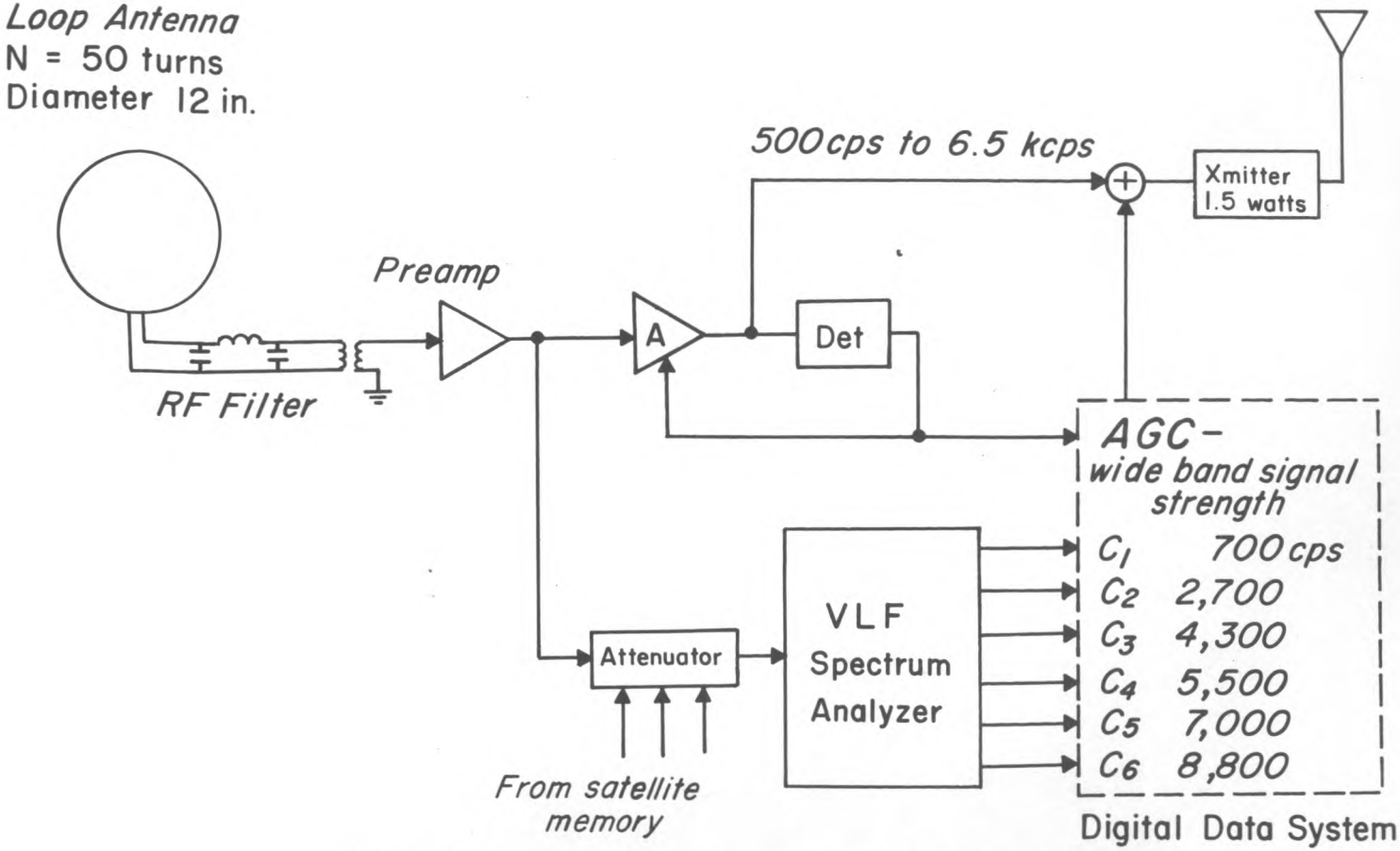

INJUN III VLF EXPERIMENT

Figure 4

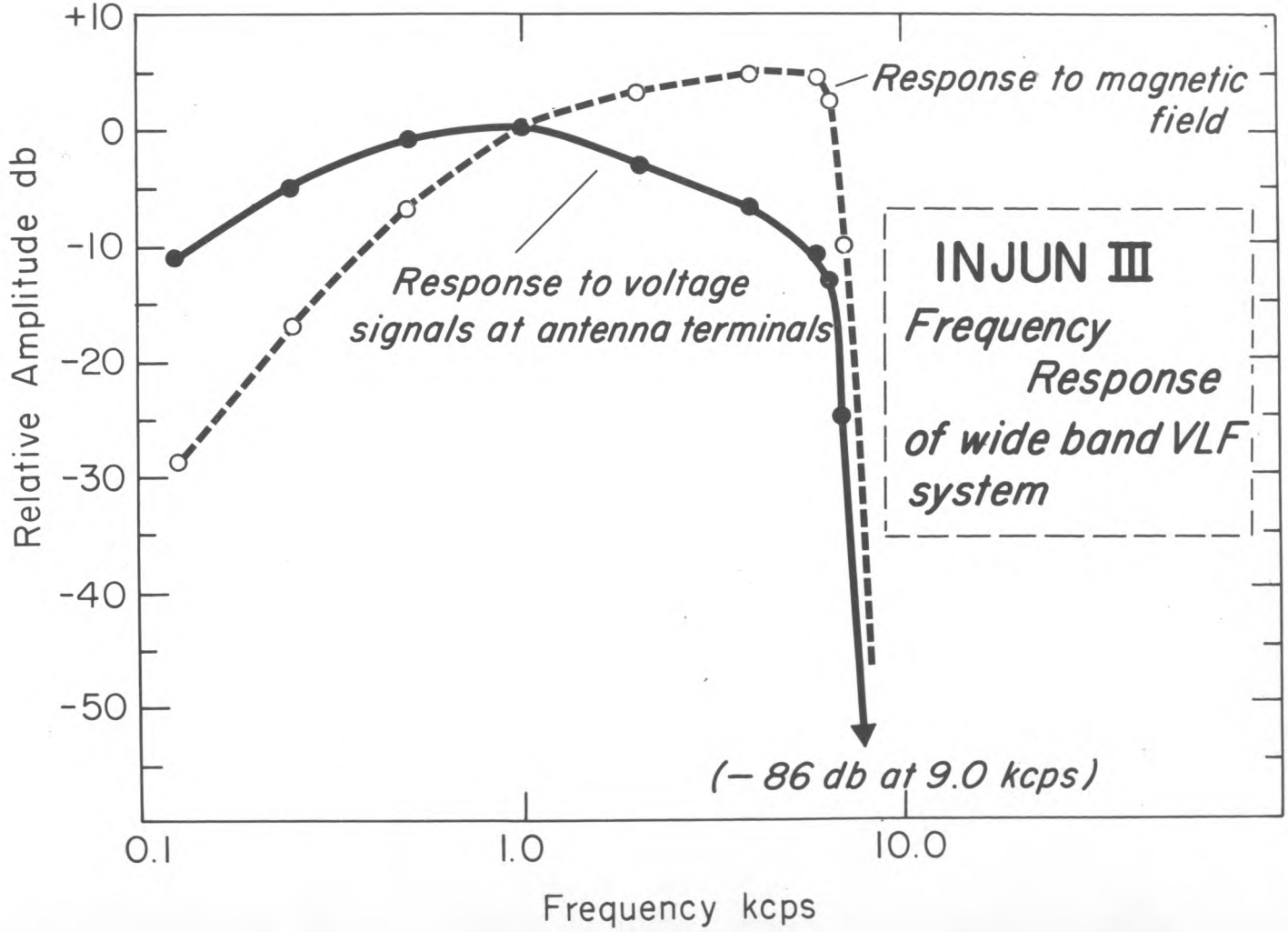
+10
0
-10
-20
-30
-40
-50
Relative Amplitude db
0.1
1.0
10.0
Frequency kcps
Response to magnetic field
Response to voltage signals at antenna terminals
INJUN III
Frequency Response of wide band VLF system
(– 86 db at 9.0 kcps)

Figure 5

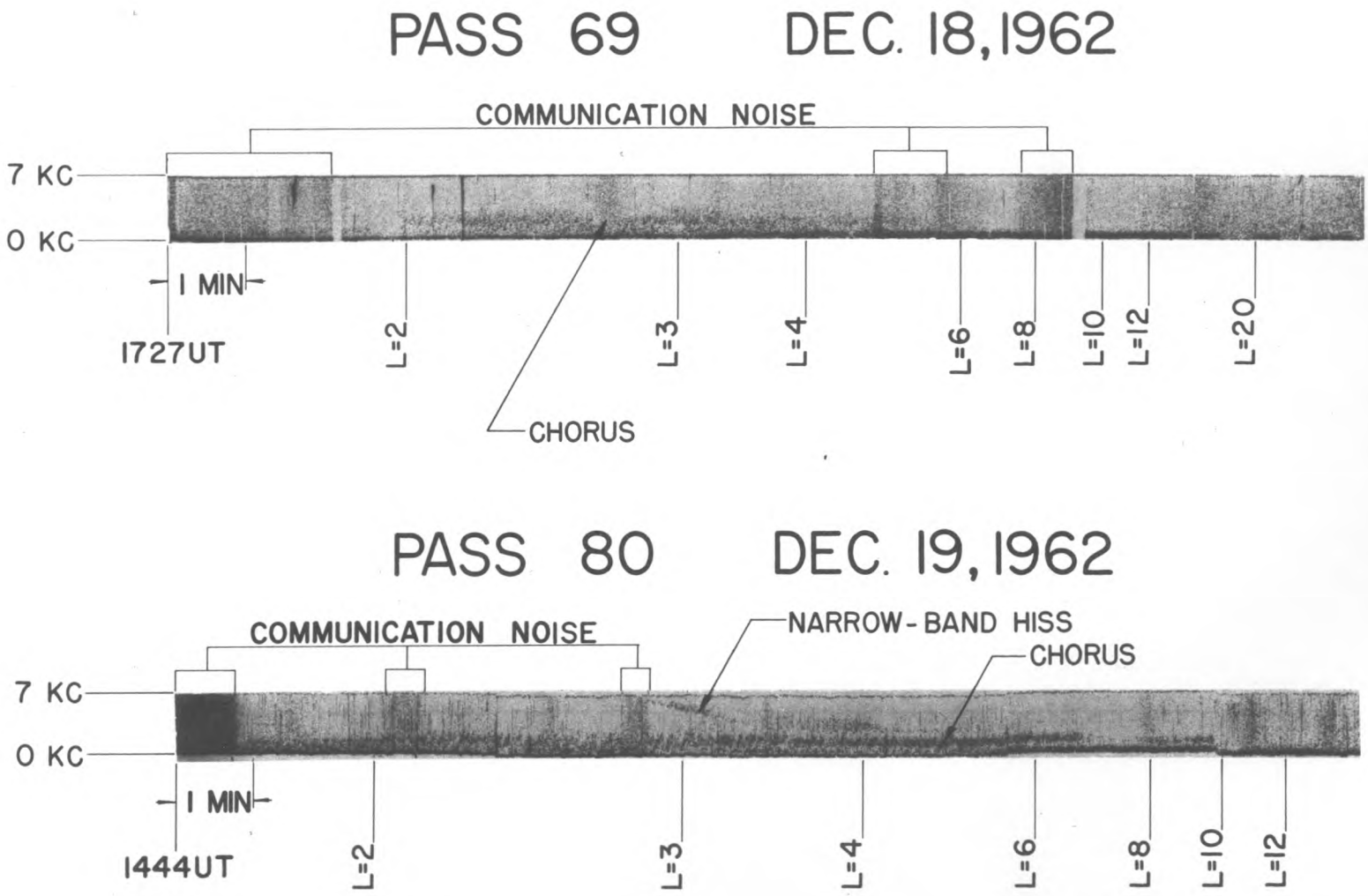
PASS 69 DEC. 18, 1962
COMMUNICATION NOISE
7 KC
0 KC
1 MIN
1727UT
L=2
L=3
L=4
L=6
L=8
L=10
L=12
L=20
CHORUS
PASS 80 DEC. 19, 1962
COMMUNICATION NOISE
NARROW-BAND HISS
CHORUS
7 KC
0 KC
1 MIN
1444UT
L=2
L=3
L=4
L=6
L=8
L=10
L=12

Figure 6

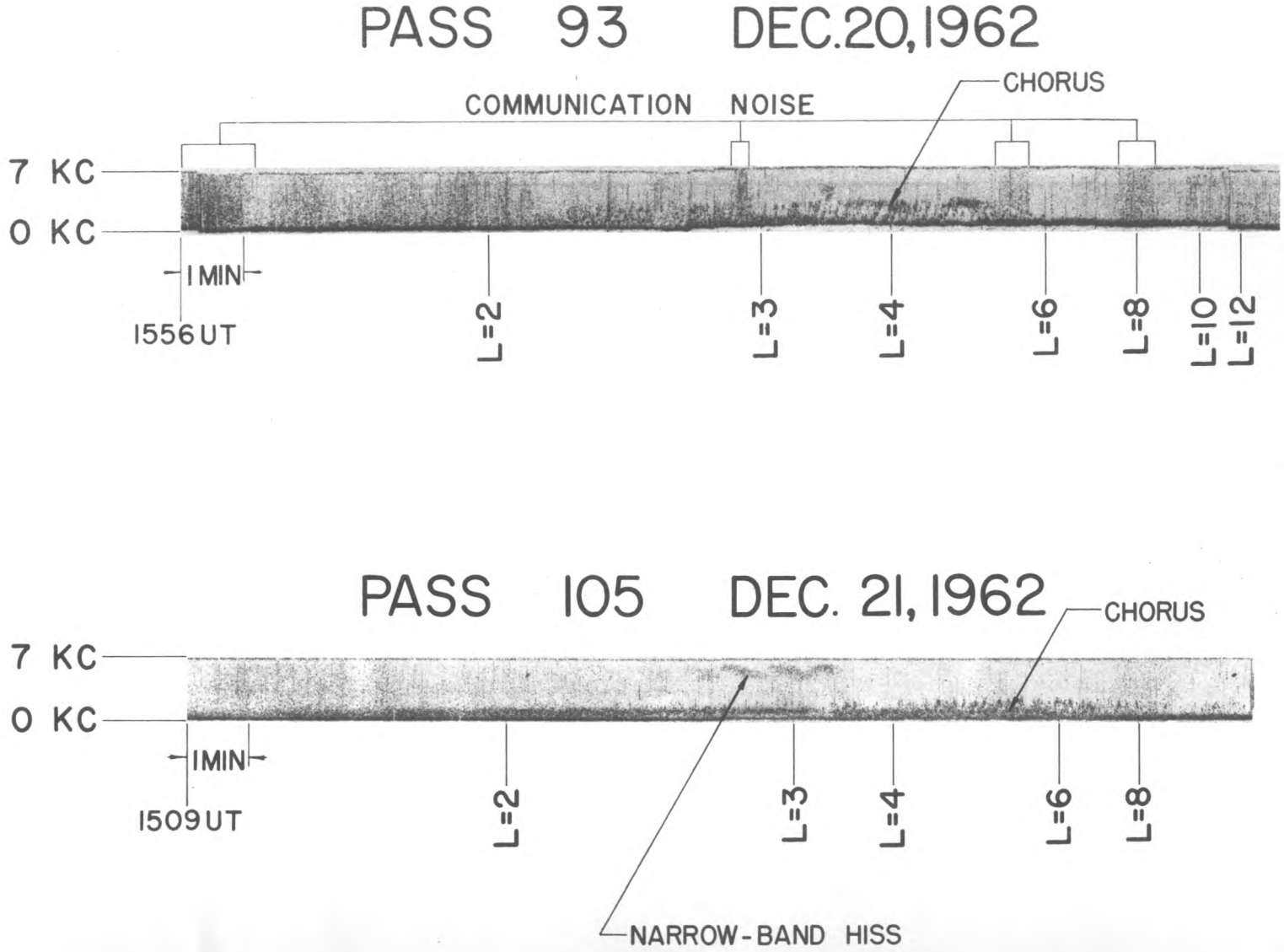
PASS 93 DEC.20,1962
COMMUNICATION NOISE
CHORUS
7 KC
0 KC
1 MIN
1556 UT
L=2
L=3
L=4
L=6
L=8
L=10
L=12
PASS 105 DEC. 21, 1962
CHORUS
7 KC
0 KC
1 MIN
1509 UT
L=2
L=3
L=4
L=6
L=8
NARROW-BAND HISS

Figure 7

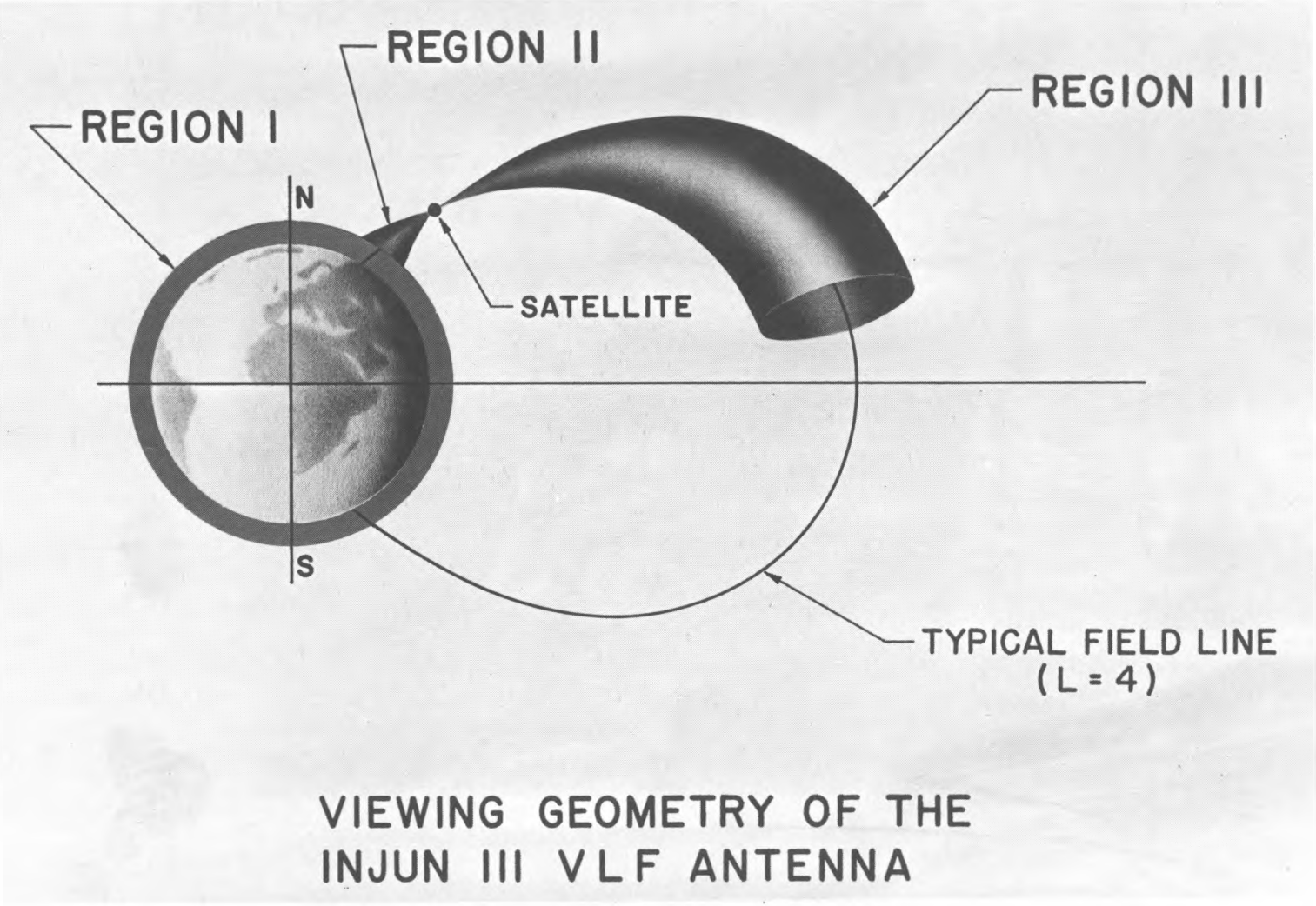
REGION II
REGION III
REGION I
N
SATELLITE
S
TYPICAL FIELD LINE
(L = 4)
VIEWING GEOMETRY OF THE
INJUN III VLF ANTENNA

Figure 8

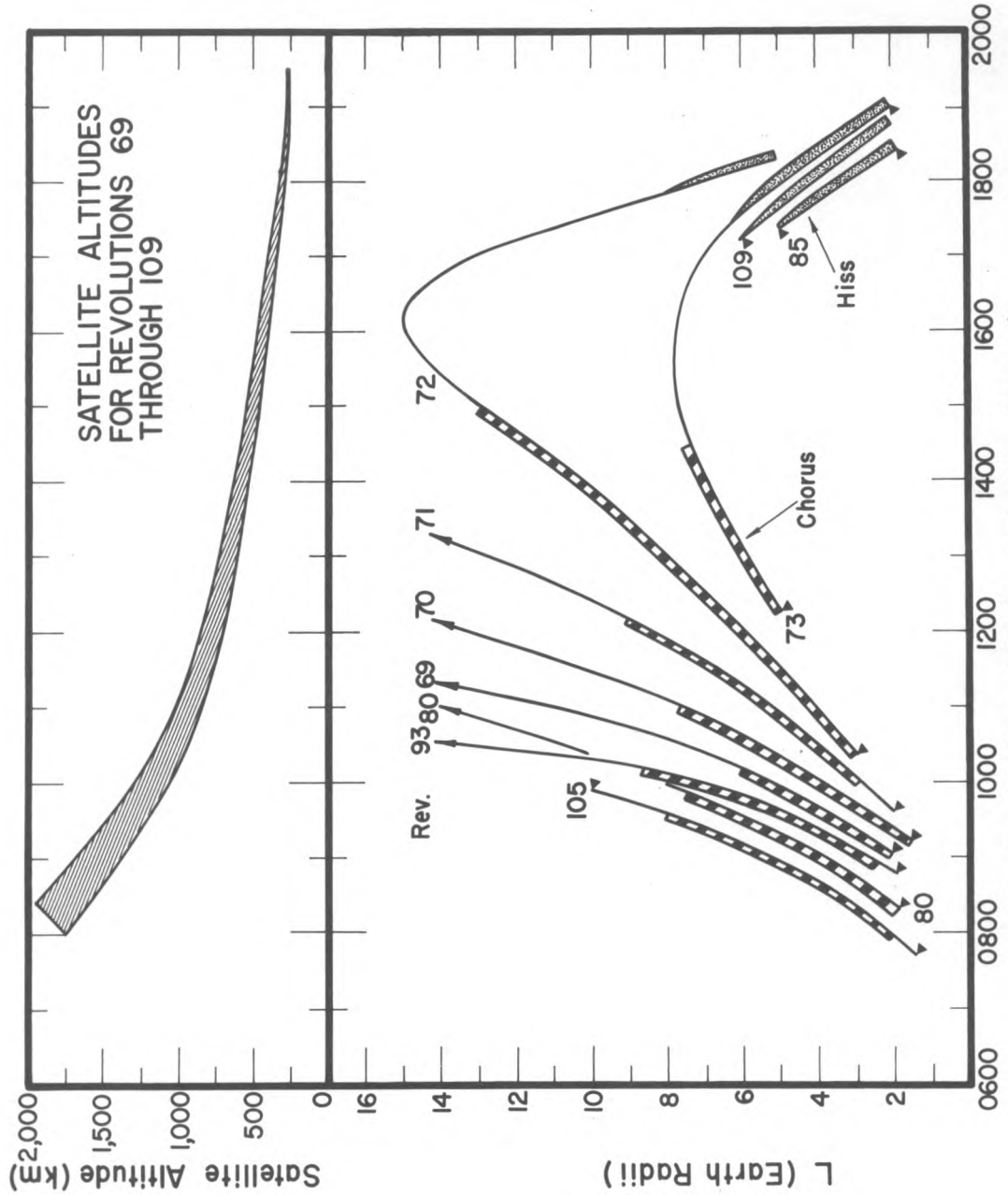
SATELLITE ALTITUDES
FOR REVOLUTIONS 69
THROUGH 109
Satellite Altitude (km)
2,000
1,500
1,000
500
0
L (Earth Radii)
16
14
12
10
8
6
4
2
0600
0800
1000
1200
1400
1600
1800
2000
Local Time At The Satellite (Hours)
Rev.
93
80
69
70
71
72
105
80
73
Chorus
109
85
Hiss

Figure 9

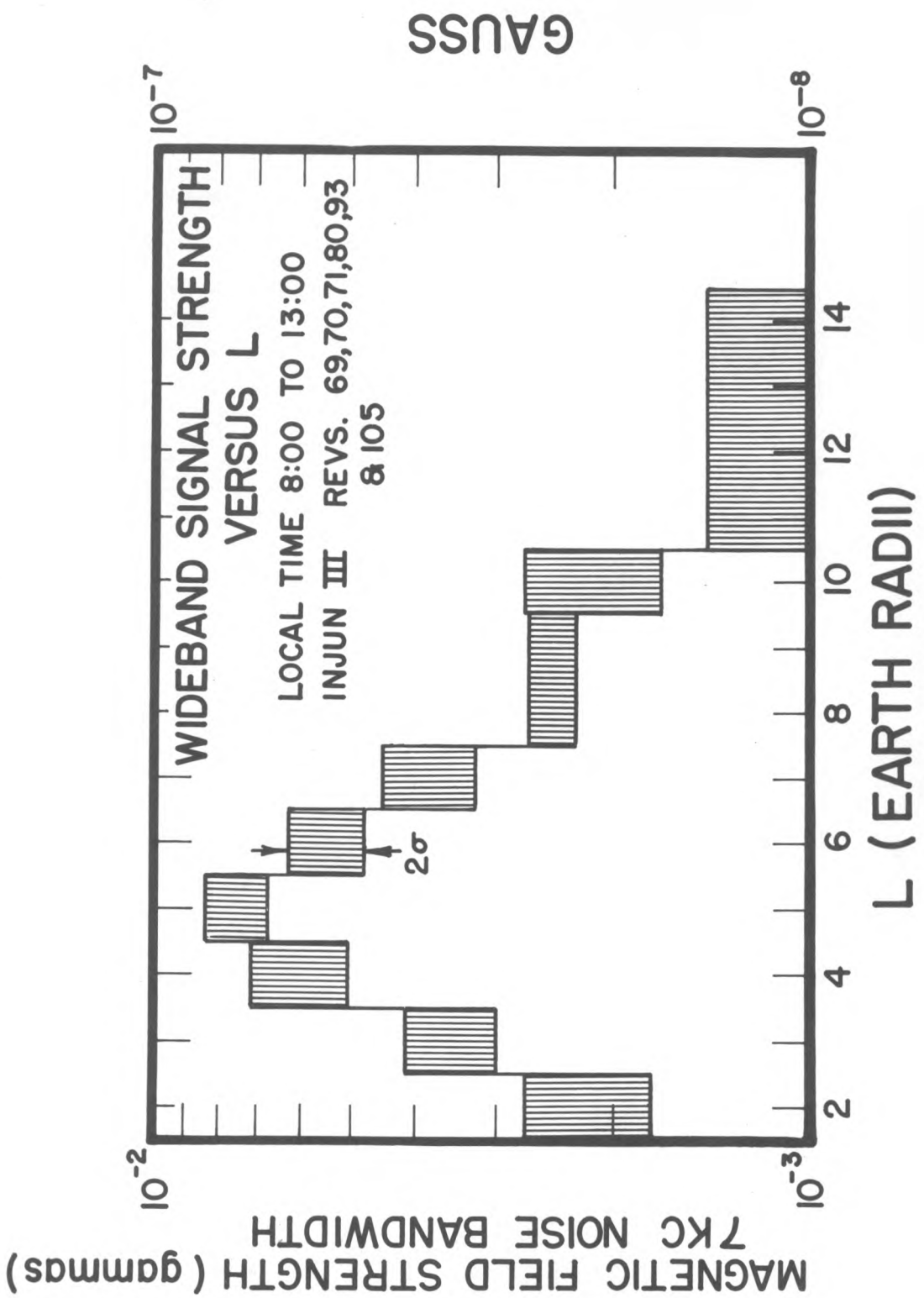
WIDEBAND SIGNAL STRENGTH
VERSUS L
LOCAL TIME 8:00 TO 13:00
INJUN III REVS. 69,70,71,80,93
& 105
2σ
L (EARTH RADII)
MAGNETIC FIELD STRENGTH (gammas)
7KC NOISE BANDWIDTH
GAUSS
10^-2
10^-3
10^-7
10^-8
2
4
6
8
10
12
14

Figure 10

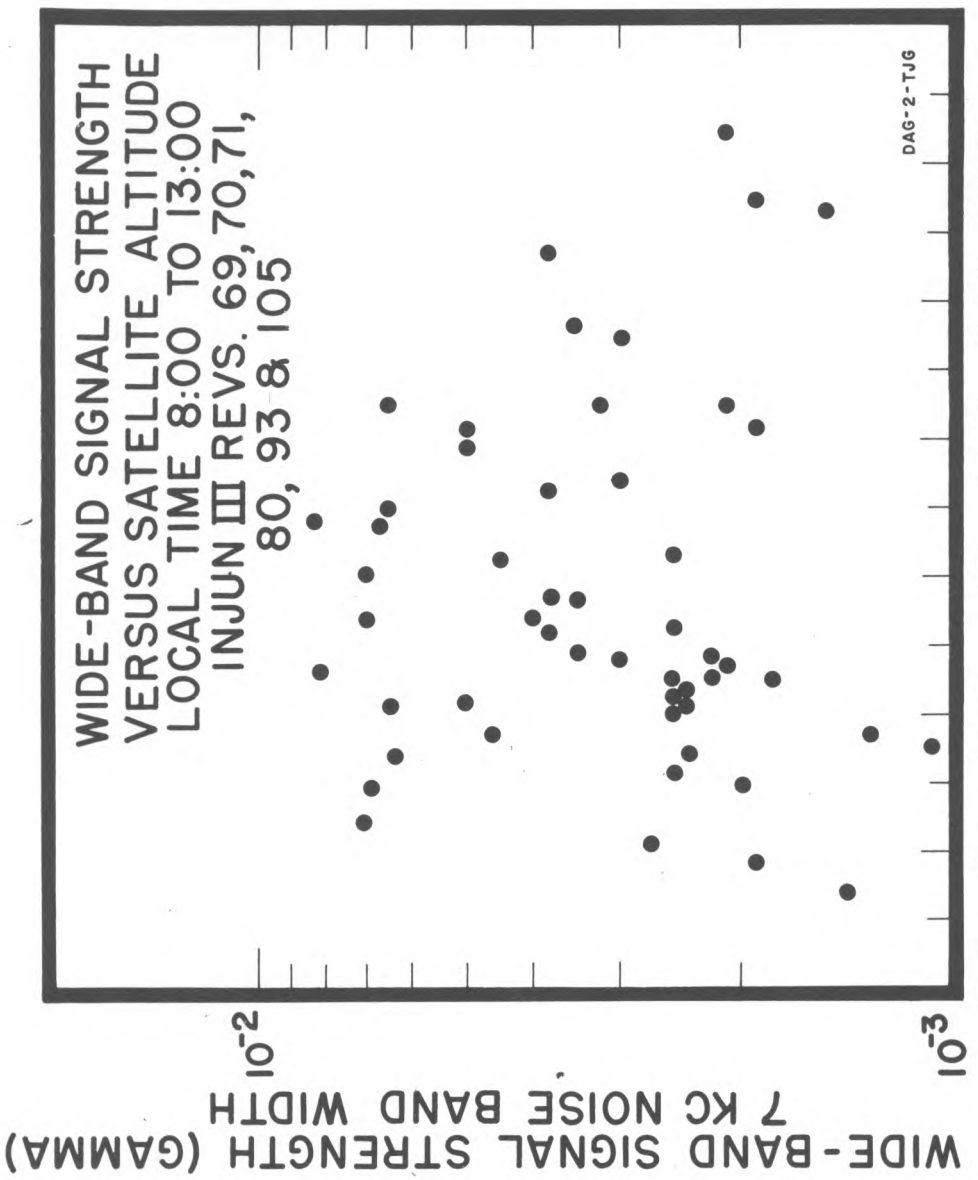
WIDE-BAND SIGNAL STRENGTH
VERSUS SATELLITE ALTITUDE
LOCAL TIME 8:00 TO 13:00
INJUN III REVS. 69, 70, 71,
80, 93 & 105
DAG-2-TJG
WIDE-BAND SIGNAL STRENGTH (GAMMA)
7 KC NOISE BAND WIDTH
10^{-2}
10^{-3}
600
800
1000
1200
1400
1600
1800
SATELLITE ALTITUDE (KM)

Figure 11

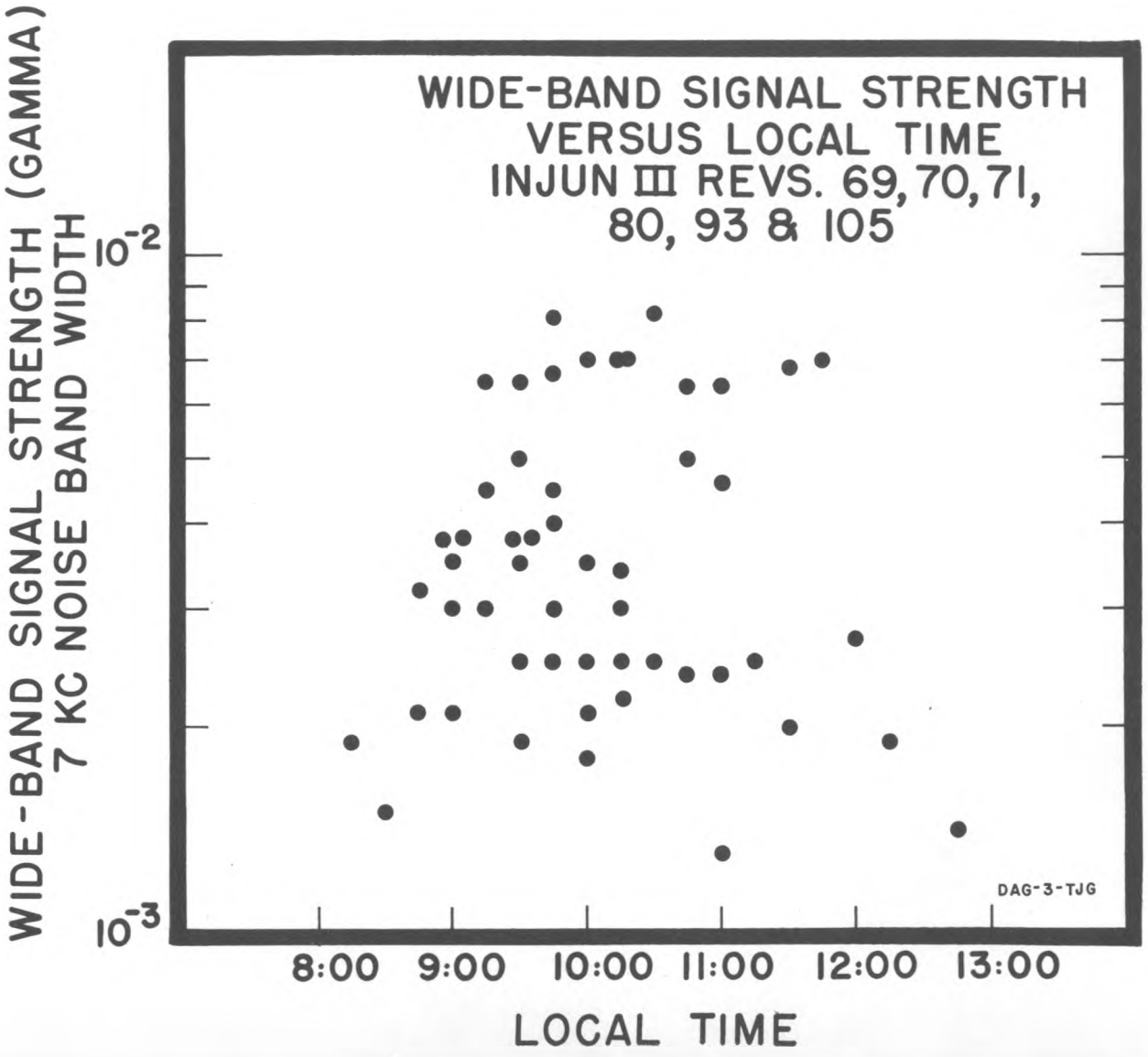
WIDE-BAND SIGNAL STRENGTH
VERSUS LOCAL TIME
INJUN III REVS. 69, 70, 71,
80, 93 & 105
WIDE-BAND SIGNAL STRENGTH (GAMMA)
7 KC NOISE BAND WIDTH
10^{-2}
10^{-3}
8:00
9:00
10:00
11:00
12:00
13:00
LOCAL TIME
DAG-3-TJG

Figure 12

BANDED CHORUS AT DIFFERENT L VALUES

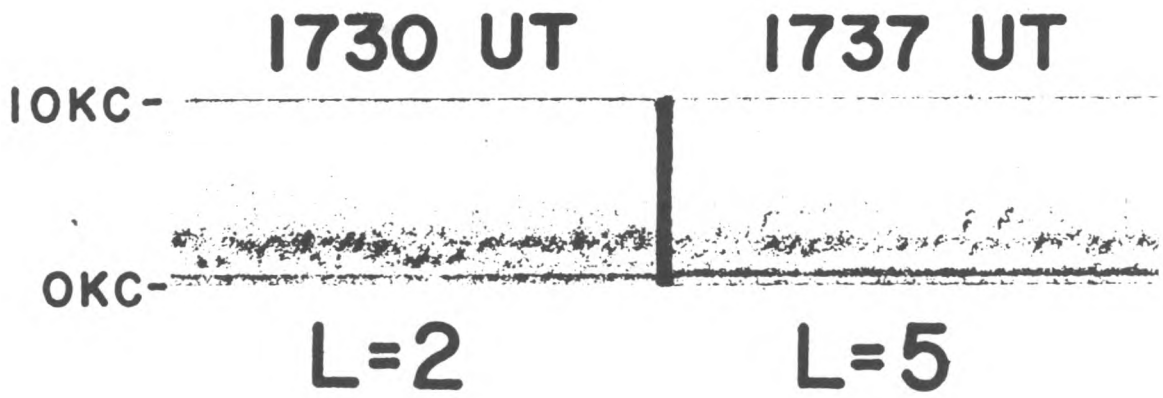

Figure 13

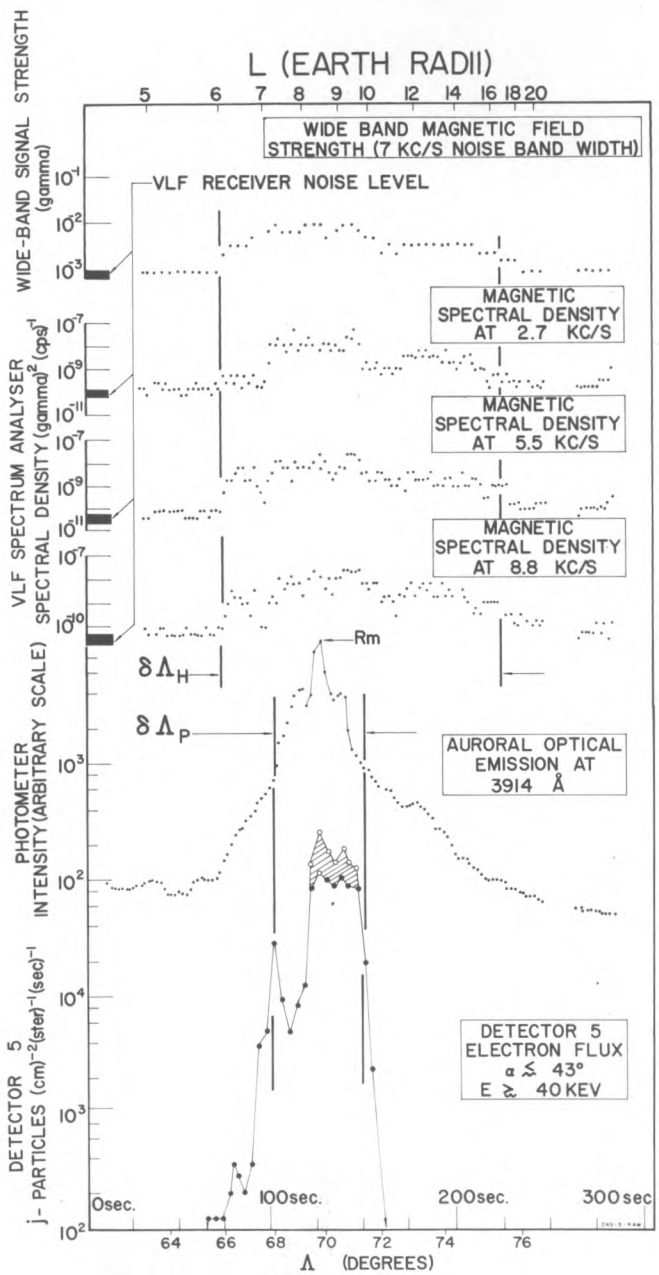

A SIMULTANEOUS OBSERVATION OF VLF ELECTROMAGNETIC EMISSION, AURORAL OPTICAL EMISSION, AND PRECIPITATED ELECTRONS 0720 TO 0725 UT MARCH 3, 1963

Figure 14

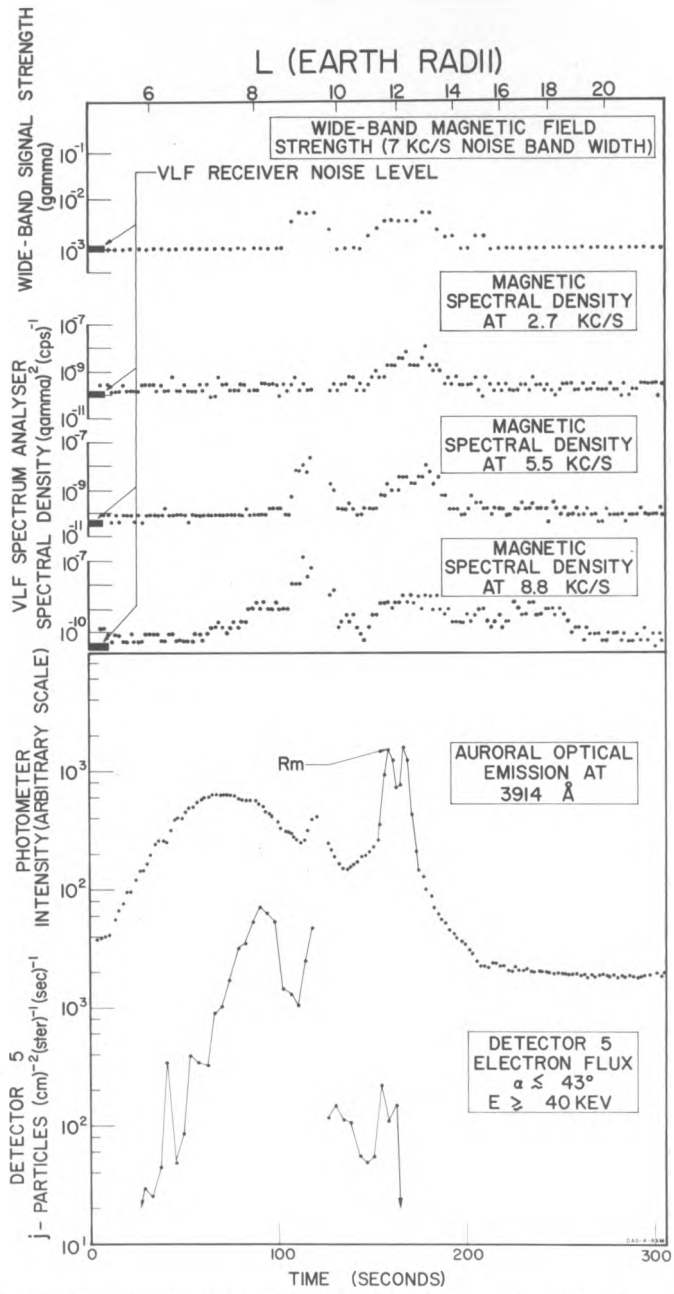

A SIMULTANEOUS OBSERVATION OF VLF ELECTROMAGNETIC EMISSION, AURORAL OPTICAL EMISSION, AND PRECIPITATED ELECTRONS 0949 TO 0954 UT FEBRUARY 28, 1963

Figure 15

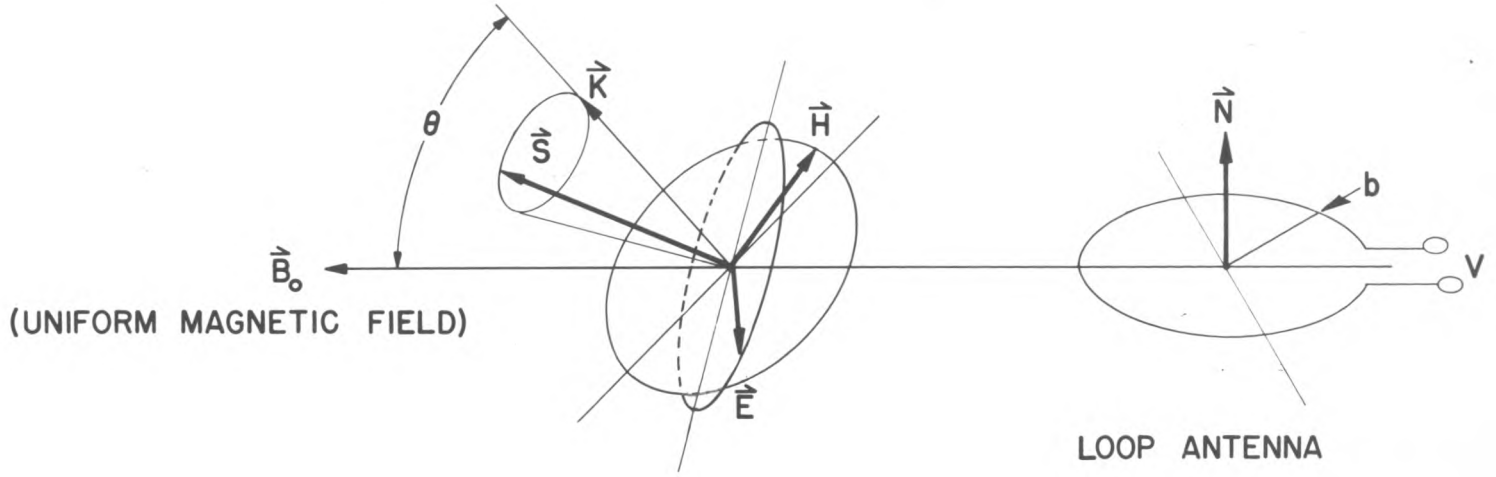

$\vec{K} \cdot \vec{H} = 0 \quad \vec{S} = \vec{E} \times \vec{H}$

ELECTROMAGNETIC FIELD AND LOOP ANTENNA GEOMETRY IN A PLASMA

Figure 16

DAG-16-RAM

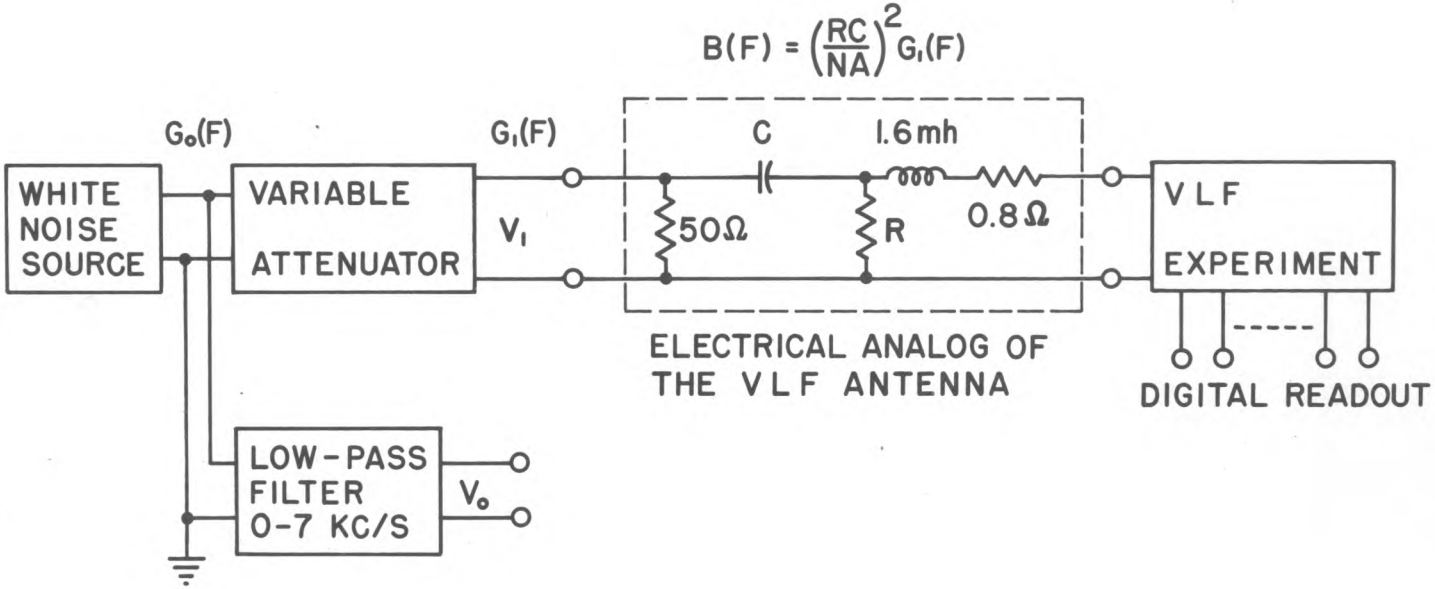

VLF EXPERIMENT CALIBRATION

dag-17-edl

Figure 17

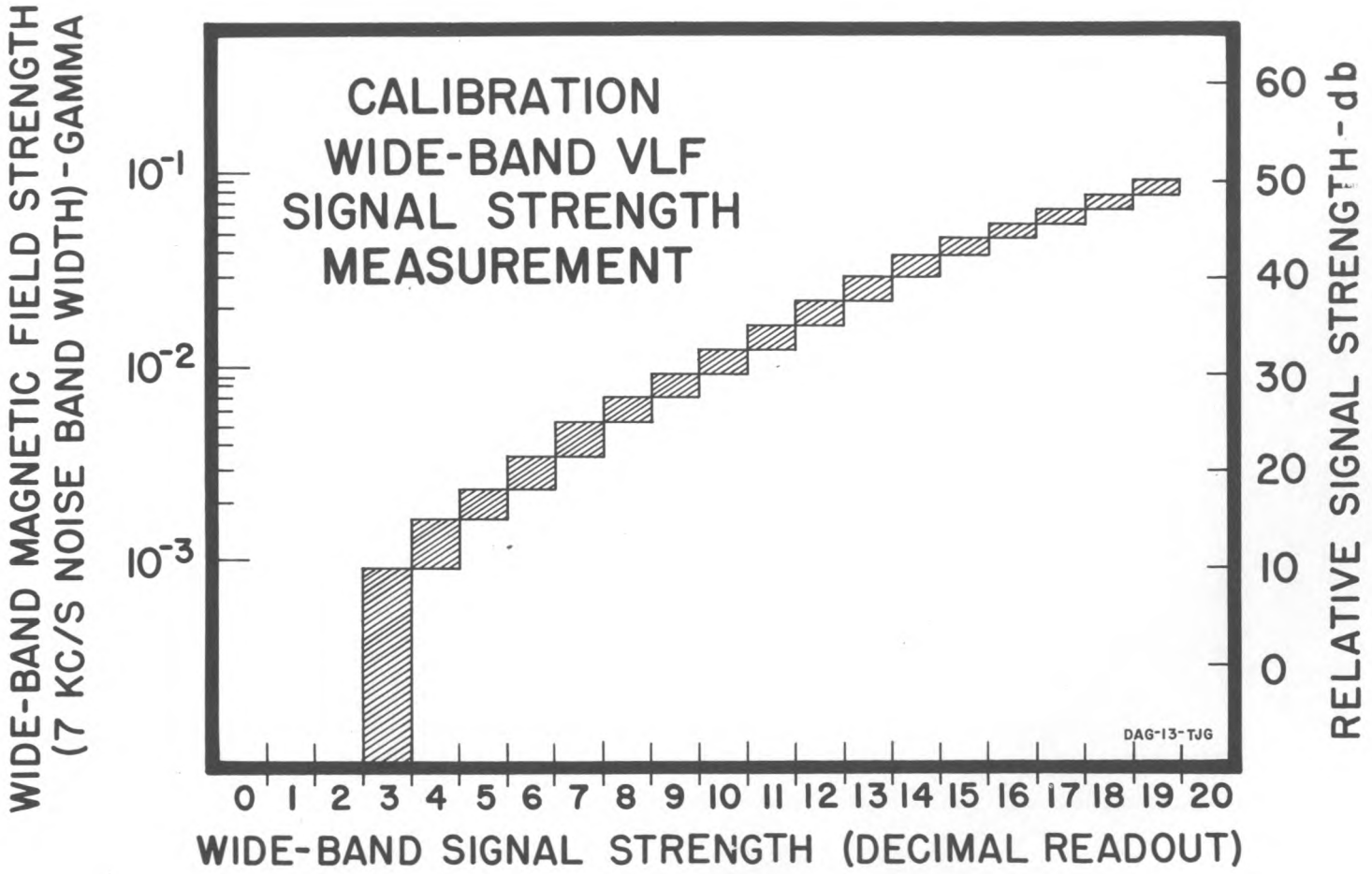
CALIBRATION
WIDE-BAND VLF
SIGNAL STRENGTH
MEASUREMENT
WIDE-BAND MAGNETIC FIELD STRENGTH
(7 KC/S NOISE BAND WIDTH)-GAMMA
10^{-1}
10^{-2}
10^{-3}
RELATIVE SIGNAL STRENGTH-db
60
50
40
30
20
10
0
DAG-13-TJG
0 1 2 3 4 5 6 7 8 9 10 11 12 13 14 15 16 17 18 19 20
WIDE-BAND SIGNAL STRENGTH (DECIMAL READOUT)

Figure 18

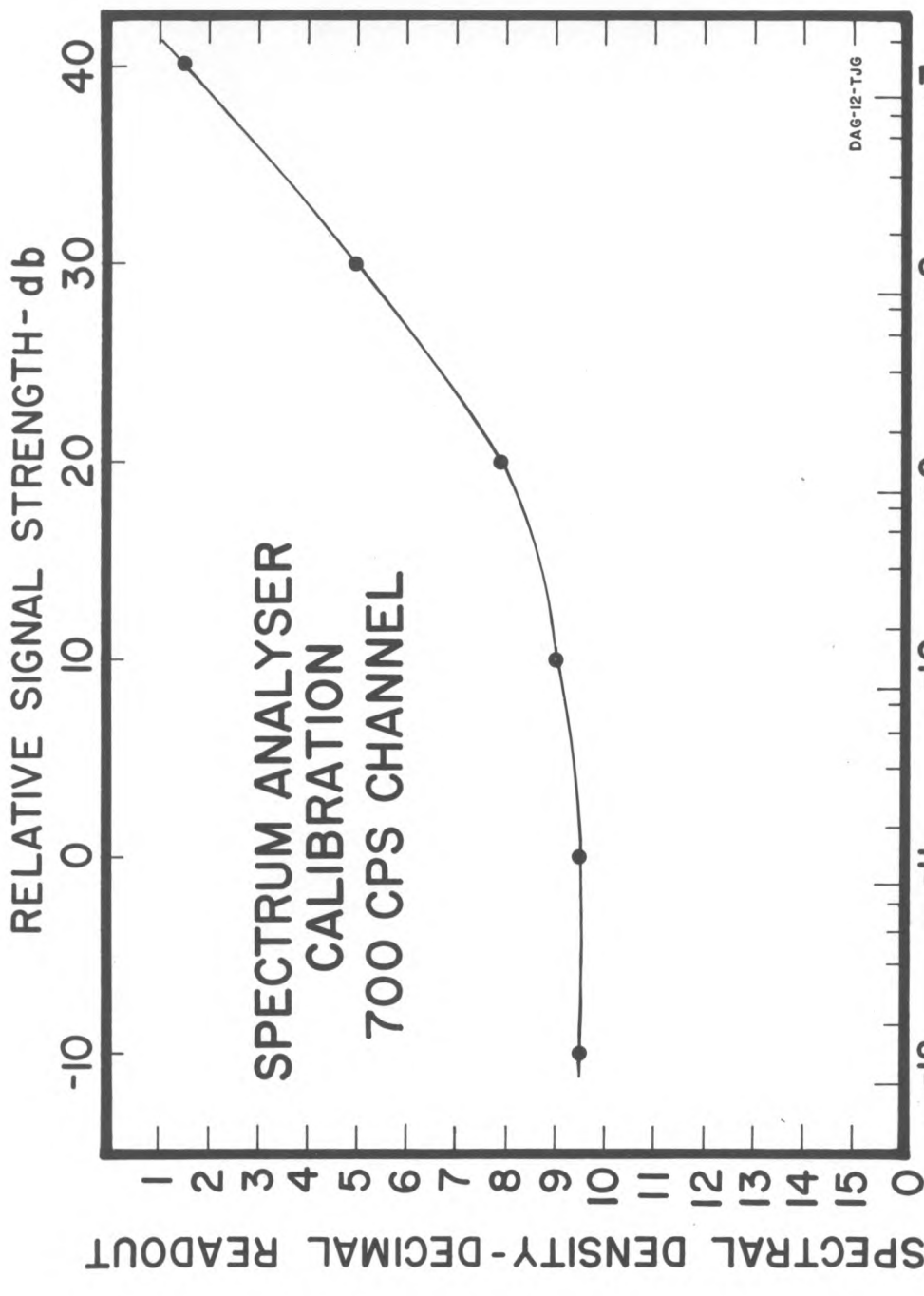
SPECTRUM ANALYSER
CALIBRATION
700 CPS CHANNEL
RELATIVE SIGNAL STRENGTH - db
-10
0
10
20
30
40
SPECTRAL DENSITY - DECIMAL READOUT
0
1
2
3
4
5
6
7
8
9
10
11
12
13
14
15
MAGNETIC SPECTRAL DENSITY (GAMMA)^2 (CPS)$^{-1}$
10^{-12}
10^{-11}
10^{-10}
10^{-9}
10^{-8}
10^{-7}
DAG-12-TJG

Figure 19

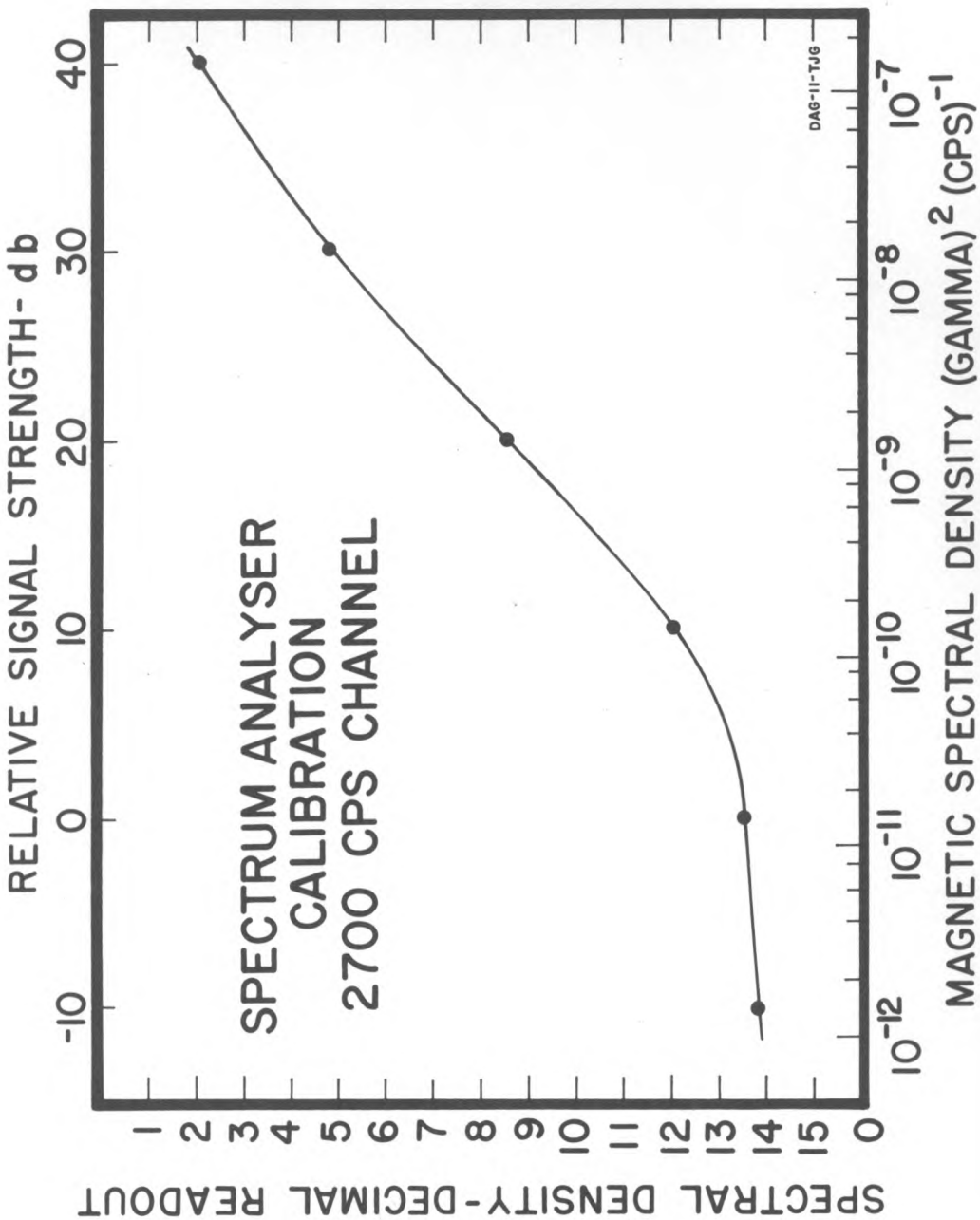
SPECTRUM ANALYSER
CALIBRATION
2700 CPS CHANNEL
RELATIVE SIGNAL STRENGTH- db
-10
0
10
20
30
40
SPECTRAL DENSITY-DECIMAL READOUT
1
2
3
4
5
6
7
8
9
10
11
12
13
14
15
0
MAGNETIC SPECTRAL DENSITY (GAMMA)^2 (CPS)$^{-1}$
10^{-12}
10^{-11}
10^{-10}
10^{-9}
10^{-8}
10^{-7}
DAG-11-TJG

Figure 20

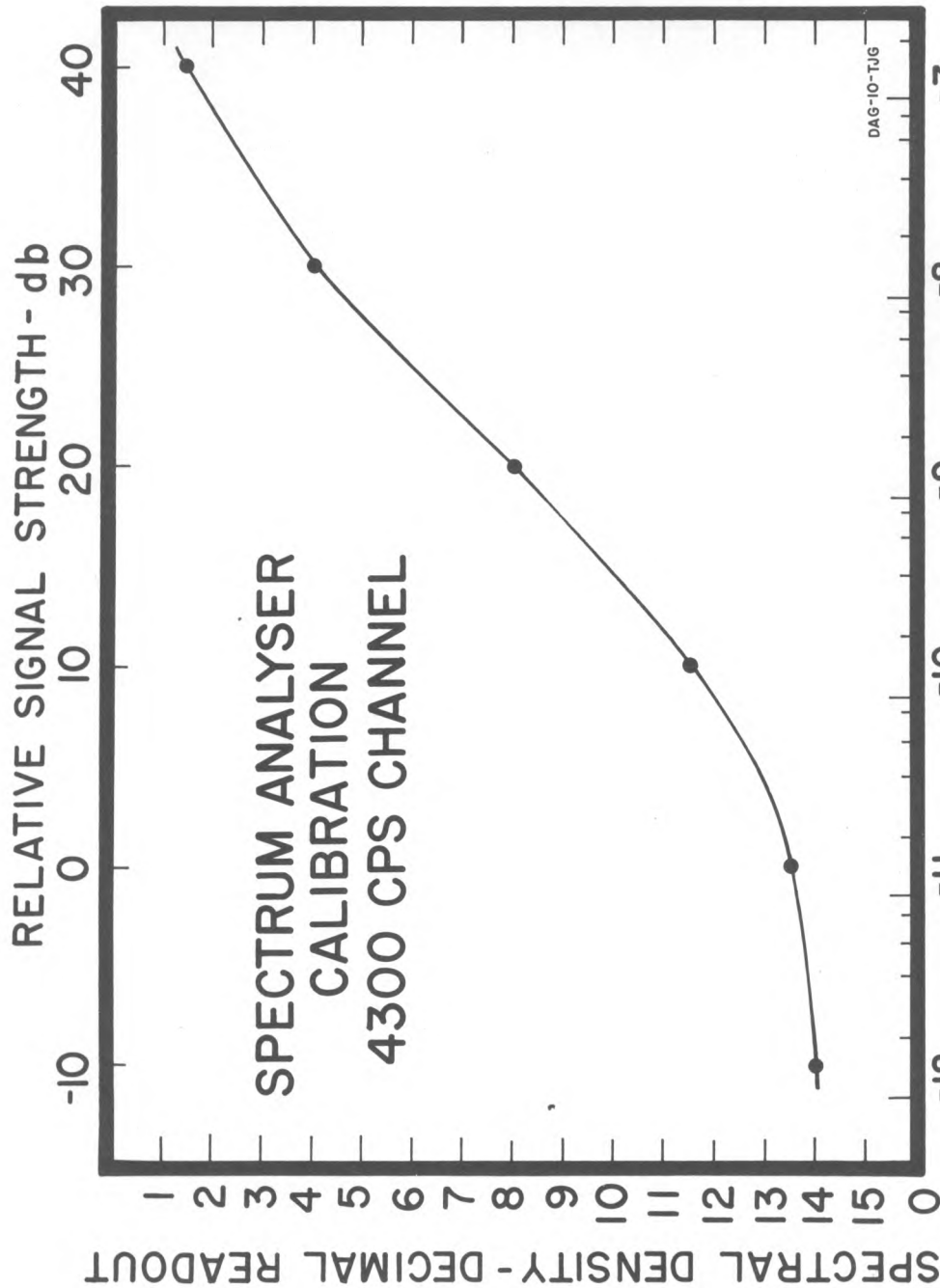
SPECTRUM ANALYSER
CALIBRATION
4300 CPS CHANNEL
RELATIVE SIGNAL STRENGTH - db
-10
0
10
20
30
40
SPECTRAL DENSITY - DECIMAL READOUT
1
2
3
4
5
6
7
8
9
10
11
12
13
14
15
0
MAGNETIC SPECTRAL DENSITY (GAMMA)^2 (CPS)$^{-1}$
10^{-12}
10^{-11}
10^{-10}
10^{-9}
10^{-8}
10^{-7}
DAG-10-TJG

Figure 21

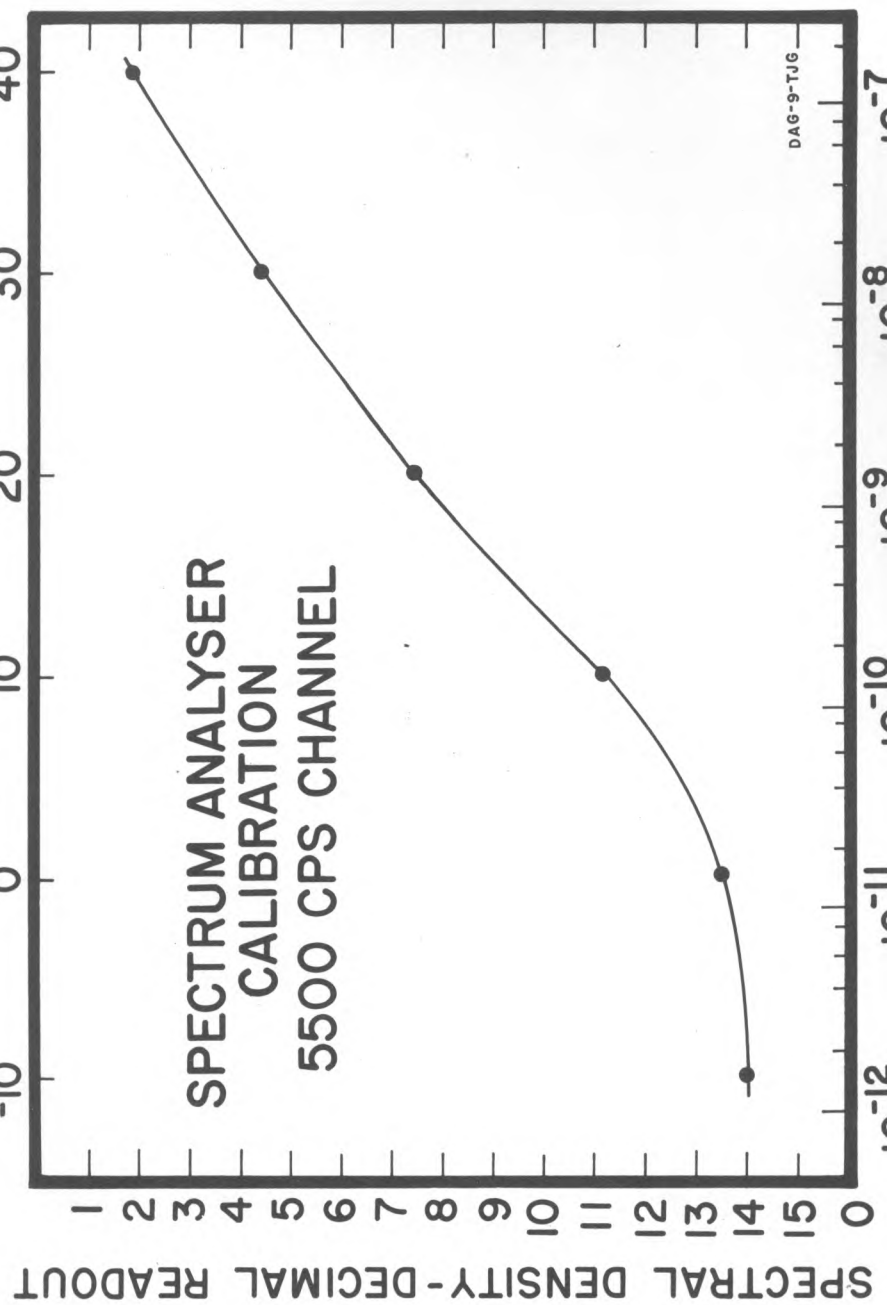
RELATIVE SIGNAL STRENGTH - db
-10
0
10
20
30
40
SPECTRUM ANALYSER
CALIBRATION
5500 CPS CHANNEL
SPECTRAL DENSITY - DECIMAL READOUT
1
2
3
4
5
6
7
8
9
10
11
12
13
14
15
0
10^{-12}
10^{-11}
10^{-10}
10^{-9}
10^{-8}
10^{-7}
MAGNETIC SPECTRAL DENSITY $(GAMMA)^2$ $(CPS)^{-1}$
DAG-9-TJG

Figure 22

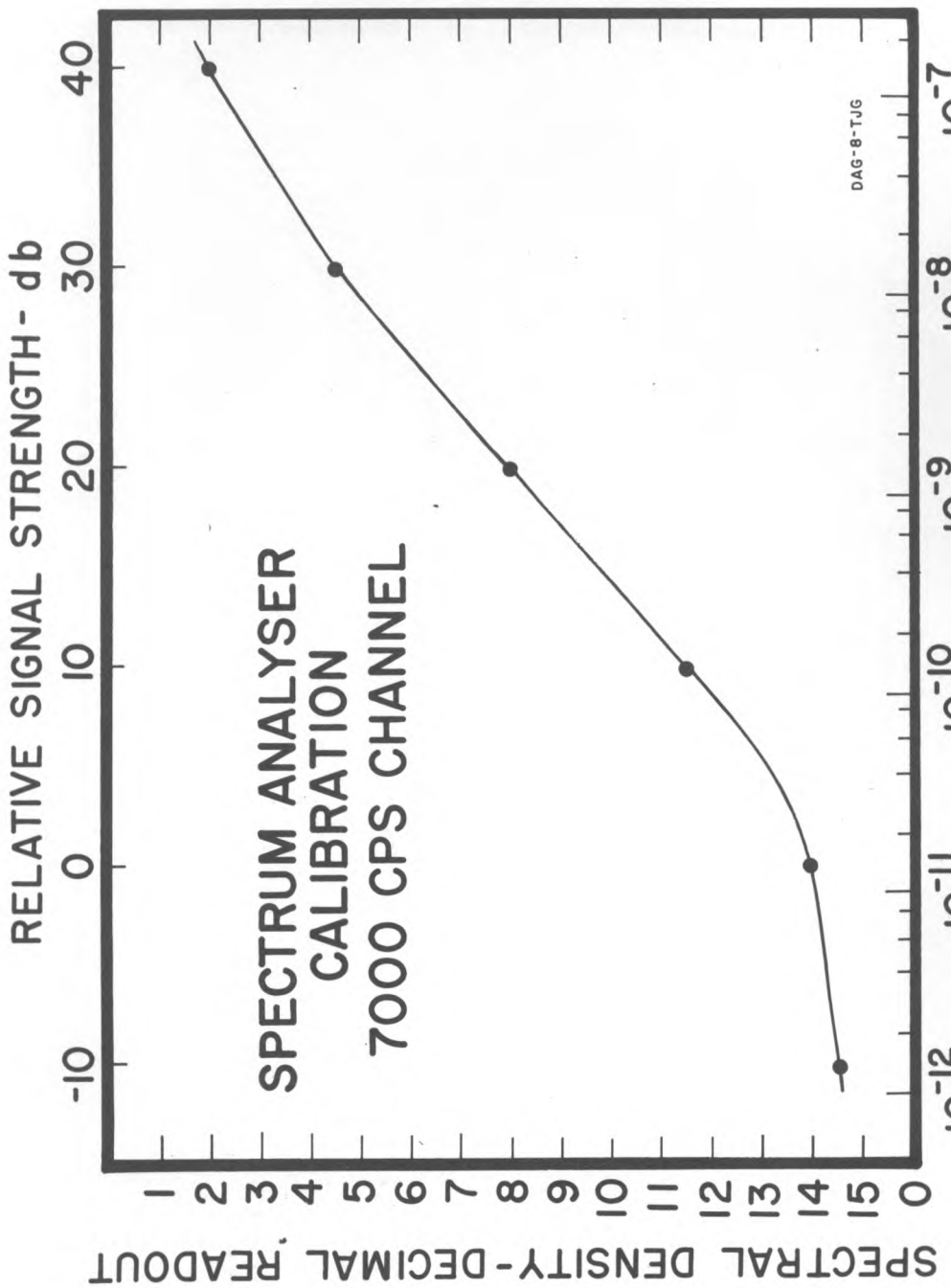
RELATIVE SIGNAL STRENGTH - db
-10
0
10
20
30
40
SPECTRUM ANALYSER
CALIBRATION
7000 CPS CHANNEL
DAG-8-TJG
SPECTRAL DENSITY - DECIMAL READOUT
1
2
3
4
5
6
7
8
9
10
11
12
13
14
15
0
10^{-12}
10^{-11}
10^{-10}
10^{-9}
10^{-8}
10^{-7}
MAGNETIC SPECTRAL DENSITY $(GAMMA)^2$ $(CPS)^{-1}$

Figure 23

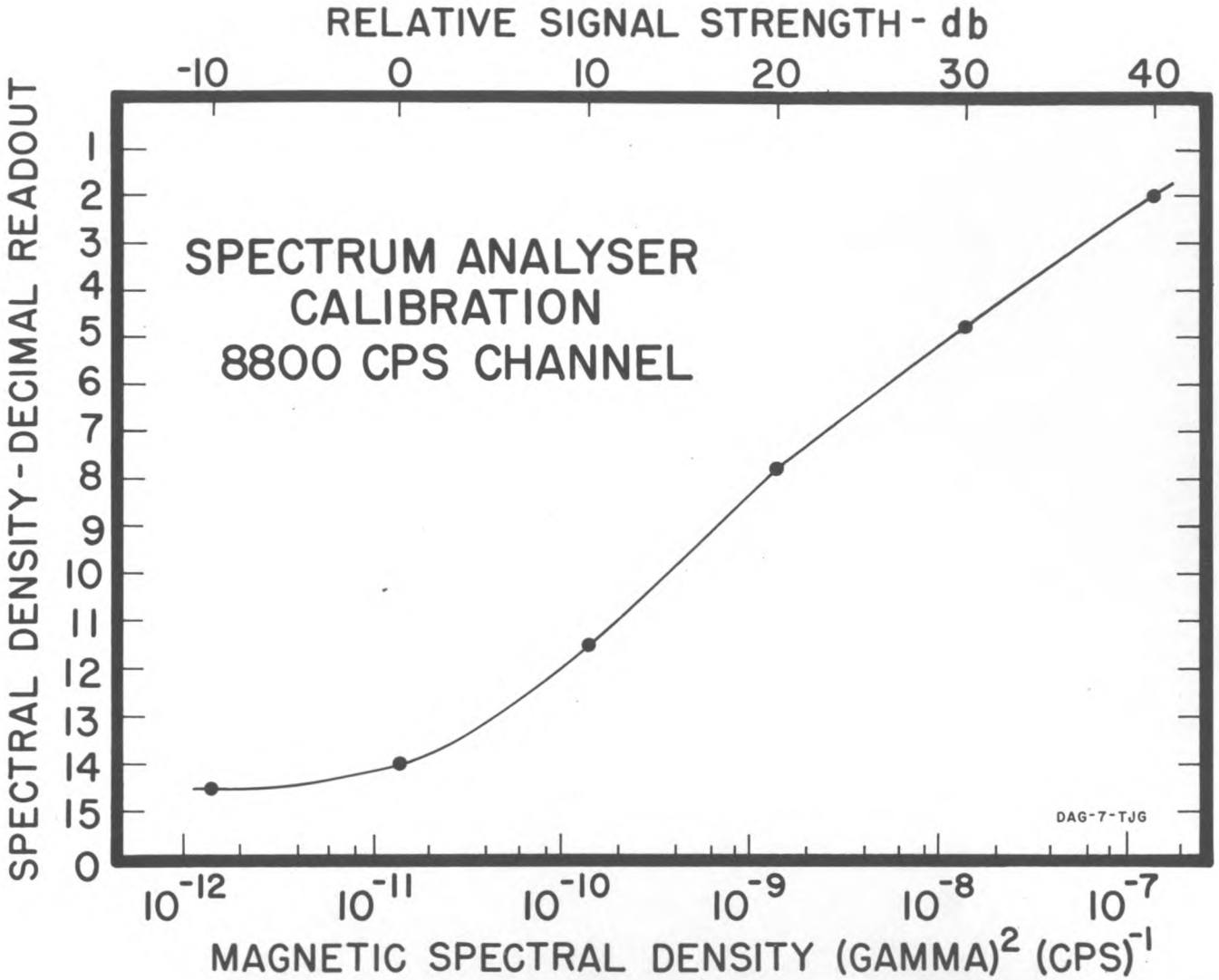
RELATIVE SIGNAL STRENGTH - db
-10
0
10
20
30
40
SPECTRAL DENSITY - DECIMAL READOUT
1
2
3
4
5
6
7
8
9
10
11
12
13
14
15
0
SPECTRUM ANALYSER
CALIBRATION
8800 CPS CHANNEL
DAG-7-TJG
10^{-12}
10^{-11}
10^{-10}
10^{-9}
10^{-8}
10^{-7}
MAGNETIC SPECTRAL DENSITY $(GAMMA)^2$ $(CPS)^{-1}$

Figure 24